

#### **OPEN ACCESS**

EDITED BY Luis Vidali,

Worcester Polytechnic Institute, United States

REVIEWED BY

Carolyn Rasmussen, University of California, Riverside, United States Han Tang, National Chung Hsing University, Taiwan

\*CORRESPONDENCE
Elena Kozgunova
Kozgunova@gmail.com

RECEIVED 25 June 2025 REVISED 30 October 2025 ACCEPTED 11 November 2025 PUBLISHED 03 December 2025

#### CITATION

Maekawa K, van Gessel N, Reski R and Kozgunova E (2025) CRISPR/Cas9 targeted genetic screening in Physcomitrella identifies novel cell division genes. *Front. Plant Sci.* 16:1653765. doi: 10.3389/fpls.2025.1653765

#### COPYRIGHT

© 2025 Maekawa, van Gessel, Reski and Kozgunova. This is an open-access article distributed under the terms of the Creative Commons Attribution License (CC BY). The use, distribution or reproduction in other forums is permitted, provided the original author(s) and the copyright owner(s) are credited and that the original publication in this journal is cited, in accordance with accepted academic practice. No use, distribution or reproduction is permitted which does not comply with these terms.

# CRISPR/Cas9 targeted genetic screening in Physcomitrella identifies novel cell division genes

Koshi Maekawa<sup>1,2</sup>, Nico van Gessel<sup>3</sup>, Ralf Reski<sup>3,4</sup> and Elena Kozgunova<sup>2,3,5</sup>\*

<sup>1</sup>School of Life Science and Technology, Institute of Science Tokyo, Tokyo, Japan, <sup>2</sup>Division of Biological Science, Graduate School of Science, Nagoya University, Nagoya, Japan, <sup>3</sup>Plant Biotechnology, Faculty of Biology, University of Freiburg, Freiburg, Germany, <sup>4</sup>Signalling Research Centres BIOSS and CIBSS, Freiburg, Germany, <sup>5</sup>Institute for Advanced Research, Nagoya University, Nagoya, Japan

Although plants share core cell division mechanisms with other eukaryotes, their unique features, such as acentrosomal spindle formation and cytokinesis via the phragmoplast, suggest the existence of plant-specific genes. This study used the model bryophyte Physcomitrium patens, commonly known as Physcomitrella, to uncover such genes and employed CRISPR/Cas9-based and localization-based screening to identify novel cell division genes. Co-expression data from known mitotic genes were used to create a pool of 216 candidate genes, which were targeted for CRISPR/Cas9 screening. Frameshift mutants with division defects were characterized using high-resolution imaging and fluorophore-based protein localization. Three novel gene families—CYR (Cytokinesis-Related), LACH (Lagging Chromosome), and SpinMi (Spindle and Phragmoplast Midzone)-were identified. CYR is linked to cytokinesis defects, LACH is essential for chromosome segregation, and SpinMi localizes to the spindle and phragmoplast midzone. None of these gene families has homologs in algae, suggesting their emergence during land colonization. These findings demonstrate the utility of co-expression-guided and targeted screening for discovering genes involved in specific cellular processes and provide insights into the evolution of the plant cell division machinery.

#### KEYWORDS

CRISPR/ Cas9, genetic screen, cell division, cell division abnormalities, Physcomitrium (Physcomitrella) patens, mitosis

## Introduction

Cell division or mitosis involves accurate duplication and distribution of genetic material, followed by the separation of two daughter cells. Errors in cell division are often connected to genetic disorders, cancer, or developmental abnormalities (Gordon et al., 2012; McIntosh, 2016). In plants, like in other eukaryotes, cell division is a fundamental process necessary for growth, development, and reproduction. While plants share basic steps of cell division with other eukaryotes, there are also significant differences. For instance, most plant cells lack centrosomes, which serve as microtubule-organizing centres in animals and fungi. As a result, plant spindles are formed without centrosomes, although they remain bipolar (Yamada and Goshima, 2017; Liu and Lee, 2022). Additionally, plant cells are surrounded by rigid cell walls, and cytokinesis occurs through the formation of a cell plate assisted by a cytoskeleton array known as phragmoplast, which transports vesicles containing cell wall materials and promotes cell plate expansion (Smertenko et al., 2018; Sinclair et al., 2022). Another well-known cytoskeletal array involved in plant cell division is the preprophase band (PPB), which forms before nuclear envelope breakdown (NEBD) and disappears shortly thereafter. This leaves behind a cortical division zone enriched with proteins that guide the phragmoplast during cytokinesis toward the site of cell division (Rasmussen and Bellinger, 2018; Yi and Goshima, 2022; Yamada et al., 2025). Notably, in some bryophytes, such as the moss Physcomitrium patens, the early development of threedimensional organs does not rely on the PPB and is presumably governed by different mechanisms (Moody, 2022; Yin et al., 2025).

Land colonization by plants was one of the most transformative events in the history of life on Earth. For plants, the transition from water to land brought about dramatic changes in many aspects of biology, including cell division (Horst et al., 2016; Chater et al., 2016; Reski, 2018a; Resemann et al., 2021; Kriegshauser et al., 2021; Lüth et al., 2023; Knosp et al., 2024). It is speculated that ancestors of land plants - related to modern Streptophyte algae - divided through centripetal cleavage, lacked PPB, and their spindles included centrosomes, which also nucleate astral microtubules, a system still observed in modern species like Klebsormidium (Buschmann and Zachgo, 2016). The development of unique features of cell division in plants has likely coincided with land colonization and may have been crucial for this event. It has long been suggested that novel genes have emerged in land plants to support the changes in the cell division mechanism (Lipka et al., 2015; Rasmussen and Bellinger, 2018; Sablowski and Gutierrez, 2022).

Several plant-specific cell division genes, such as KNOLLE and FASS/TON2, have been identified through forward genetic screening (Traas et al., 1995; Lukowitz et al., 1996; Camilleri et al., 2002; Wright et al., 2009). Traditionally, forward genetic mutant collections are generated using methods such as chemical mutagenesis, physical irradiation, or insertional agents like T-DNAs and transposons. However, these approaches are often limited by the need to obtain homozygous progeny and the labour-intensive, time-consuming process of identifying causal mutations responsible

for observed phenotypes. The development of CRISPR/Cas9 geneediting technology has revolutionized targeted mutagenesis, making it more accessible and efficient. CRISPR/Cas9 has also been applied to forward genetic screening in plants (Meng et al., 2017; Liu et al., 2020).

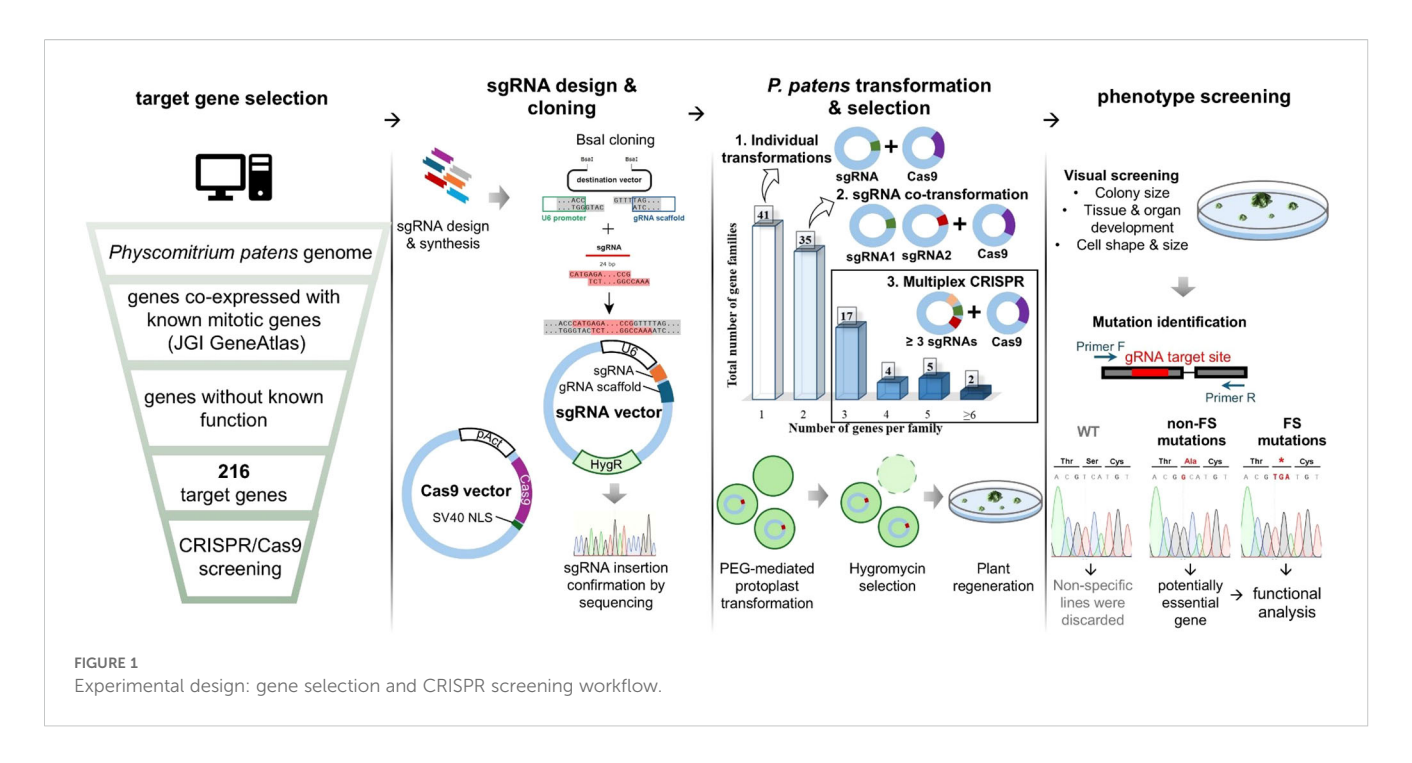
In this study, we asked if it is possible to identify novel cell division genes in plants by combining CRISPR-based genetic screening with co-expression analysis of known mitotic genes, utilizing the model bryophyte *Physcomitrium patens* (*P. patens*), also known as Physcomitrella (Lueth and Reski, 2023). *P. patens* is a widely used model in plant cell division research owing to its simple body plan, amenability for high-resolution imaging, and ease of genetic manipulation (Reski, 2018b; Rensing et al., 2020). Previous studies have functionally characterized numerous cell division genes in *P. patens*, including kinetochore genes (Kozgunova et al., 2019) and various microtubule-associated proteins (Nakaoka et al., 2012; Miki et al., 2014; Kozgunova et al., 2022).

Our central hypothesis was that genes involved in a particular cellular process, such as cell division, might share similar expression patterns. Therefore, co-expression data of known cell division genes can be leveraged to enrich a target gene pool with candidate genes likely involved in mitosis. To test this hypothesis, we extracted coexpression information from a publicly available database of 25 known mitotic genes (primarily kinetochore, microtubuleassociated and kinase genes), filtered the dataset to focus on genes with unknown functions, and subsequently used CRISPR/Cas9 for genetic screening. From the CRISPR lines, we identified a frameshift mutant with defective phragmoplast formation, resulting in prolonged mitosis and frequent cytokinesis failures. We also discovered a conserved gene family localized to the spindle and phragmoplast midzone and another gene family that is likely essential for moss viability. Knock-down of the latter with inducible RNAi resulted in a chromosome missegregation phenotype. Interestingly, all three gene families are found in land plants, with varying degrees of conservation, but not in the algae lineage. Our findings serve as a proof-of-concept of the effectiveness of targeted gene screens and leveraging co-expression information for gene discovery associated with specific biological processes.

## **Results**

# A pool of genes for targeted genetic screening

Cell division genes likely make up only a small fraction of the genome. For example, in human cells, it is estimated that approximately 2.4% to 4.25% of genes are involved in cell division (Whitfield et al., 2002; Bar-Joseph et al., 2008). Given this, we believed that a forward genetic approach is not an efficient strategy to uncover novel cell division genes and decided to pursue a targeted reverse genetic screening instead. By leveraging co-expression data, we aimed to build a pool of previously uncharacterized genes that may be involved in cell division, based on their co-expression with known mitotic genes (Figure 1).



Multiple mitotic genes, including kinetochore genes (Kozgunova, 2025), microtubule-associated proteins (Nakaoka et al., 2012; Kosetsu et al., 2013; Leong et al., 2018; Kozgunova et al., 2022) and motor proteins (Miki et al., 2014; Wu and Bezanilla, 2014) have been functionally characterized in Physcomitrella. We used the publicly available JGI Gene Atlas database to collect information on co-expression networks of selected mitotic genes (Supplementary Table 1). As an arbitrary cut-off score, we adopted a co-expression value above 0.8. To further narrow down our gene pool, we excluded genes whose function could be predicted based on homology and genes that had been functionally characterized based on publication records. In addition, we selected several Arabidopsis genes that have been reported to be highly expressed in dividing cells, either based on synchronized culture (Menges and Murray, 2002) or embryo analysis (Slane et al., 2014), but were not further characterized. We then identified homologs of these genes in Physcomitrella and included them in the screening. In total, 52 genes were selected based on the Arabidopsis studies, while the remaining 164 genes were identified through co-expression analysis. A full list of the in total 216 genes selected for screening, along with the mitotic genes they co-express with, is provided in Supplementary Table 1.

## A gRNA library and screening

Guide RNAs (gRNAs) were designed manually using the CRISPOR website (Concordet and Haeussler, 2018), targeting exon regions, typically choosing the exon that was present in all transcript variants (Supplementary Table 1). In addition, the genes were grouped based on their homology, and when possible, a single gRNA was designed to target multiple genes from a single gene family through a conserved site. gRNA expression was driven by the

U6 promoter and gRNA integration site was followed by gRNA scaffold (Lopez-Obando et al., 2016) (Figure 1). When three or more gRNAs were required to target all identified gene homologues, we performed an additional cloning step to incorporate all gRNAs into a single vector. As a background line, we chose a line expressing GFP-tubulin and H2B-RFP, which allows us to visualise microtubules and chromosomes, respectively (Nakaoka et al., 2012). Hereinafter, we refer to this line as the GH line.

# Phenotype screening and mutation mapping

After transforming the gRNA vectors into moss protoplasts, we visually assessed the phenotypes of the regenerated colonies that survived antibiotic selection. We hypothesized that defects in cell division would result in smaller colonies and abnormal cell or organ shapes. Accordingly, we selected colonies exhibiting these phenotypic characteristics and sequenced them.

Upon sequencing, we have encountered three potential outcomes:

- No mutation was detected at the gRNA target site, which was considered a non-specific result, leading to the exclusion of such colonies.
- Exclusively non-frameshift mutations were identified in multiple colonies. This outcome suggested that the targeted gene might be essential for moss viability, and in some cases, we pursued further analysis of such genes using alternative methods.
- Frameshift mutations in the gRNA target site were correlating with the observed phenotype, providing strong evidence of a functional relationship between the mutation and the phenotype.

One of the gene families was shown to have severe growth retardation after frameshift mutation (Figures 2A, B). We decided to further pursue functional characterization of this gene family.

# Cytokinesis-related (CYR) gene family affects spindle and phragmoplast

This gene family consists of two genes in P. patens and potential homologues were also found in other bryophytes, as well as in some vascular plant species. We named this gene family Cytokinesis-Related (CYR) to reflect the cellular phenotype observed in frameshift mutants, with CYR1 (version 3.3: Pp3c26\_15160; version 6.1: Pp6c26\_8300) and CYR2 (version 3.3: Pp3c4\_27710; version 6.1: Pp6c4 14480) assigned as the respective gene names. The two genes in this family encode proteins of approximately 100 kDa, with around 57% shared amino acid sequence identity and an assignment to the PANTHER family GPI-ANCHORED ADHESIN-LIKE PROTEIN (PTHR36022). Using CYR1 and CYR2 as queries we performed homology searches against a reference species set covering major lineages of Archaeplastida, including chlorophytic and charophytic algae. Careful evaluation and phylogenetic reconstruction revealed conservation of the gene family across land plants (Figure 2C), but no homologs in algae. In silico prediction of subcellular localization for both protein sequences identified no specific signal peptides, but hinted towards cytoplasmic and nuclear localization (Supplementary Table 2). In our co-expression analysis, the CYR gene family was selected based on co-expression with mitotic kinase MPS1 (Pp3c6\_320) and microtubule-associated protein TPX2-4 (Pp3c23\_4540) (Supplementary Table 1). To the best of our knowledge, this gene family has not been characterized previously.

During CRISPR screening we isolated two independent clones in which both *CYR1* and *CYR2* genes carried frameshift mutations (Supplementary Figure 1A). To assess their cellular phenotypes, we first stained the cells with FM4-64, a membrane marker, and observed incomplete cell plate formation and multinucleated cells, suggesting cytokinesis failure (Supplementary Figure 1B). High-resolution imaging of *cyr1cyr2* mutants confirmed cytokinesis failure in 2 out of 3 cells in *cyr1cyr2 #1* line and 2 out of 4 cells in *cyr1cyr2 #2* line (Supplementary Video 1). However, due to the severity of the phenotype, it was difficult to collect data from a large number of cells.

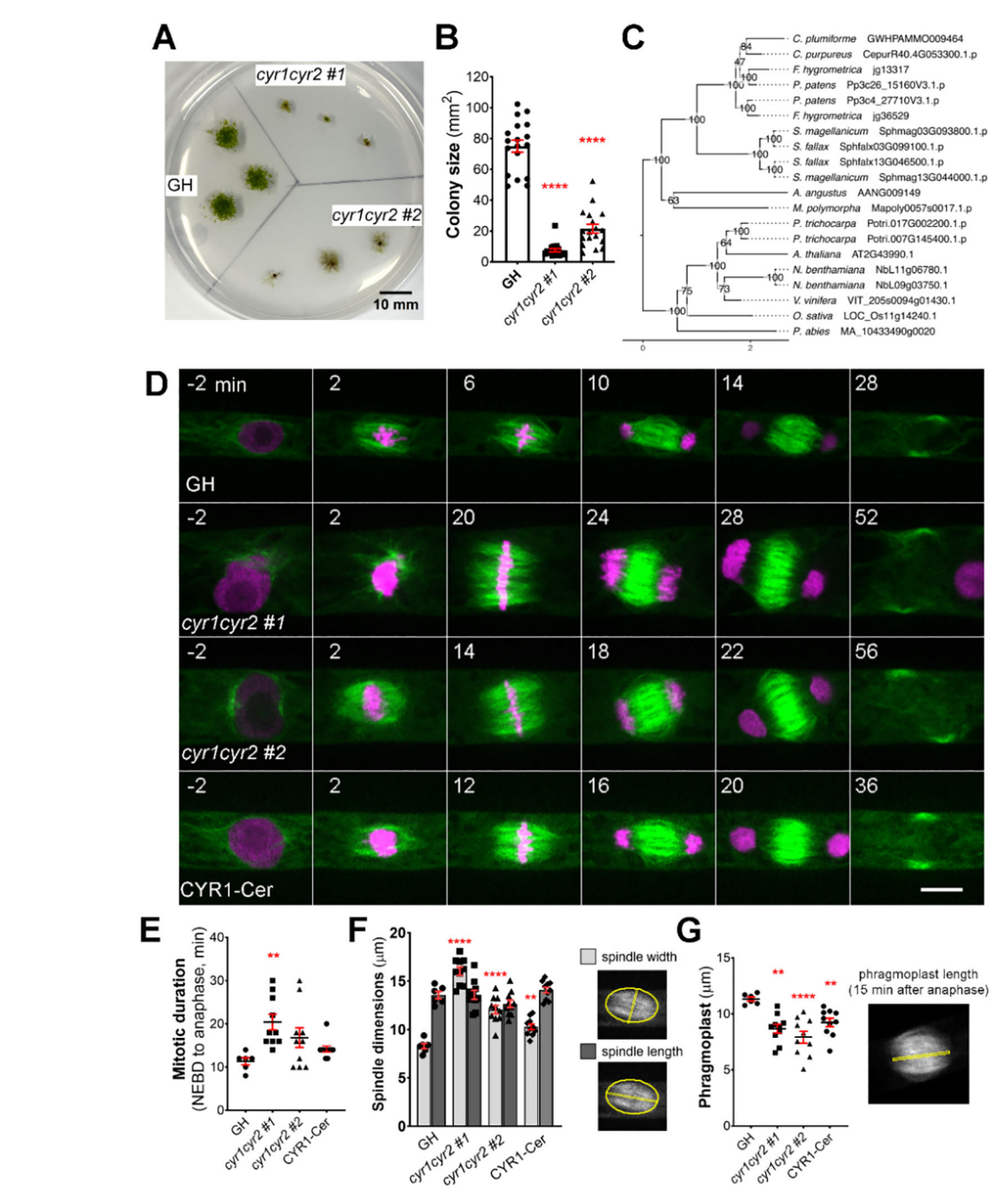
After continuous culture, the phenotype became less pronounced, possibly due to adaptive mutations, epigenetic changes, or polyploidization. In these "adapted" lines, cytokinesis failure was no longer observed during live-cell imaging. To further characterize their morphology, we repeated FM4–64 staining and quantified the frequency of abnormal phenotypes, including multinucleated cells, incomplete cell plates, multiple cell plates, and abnormal branching (Supplementary Figures 1C, D). Overall, approximately 32% of cells in the adapted *cyr1cyr2* #1 line and 47% in the adapted *cyr1cyr2* #2 line exhibited some form of abnormality. However, multinucleated cells, which typically represent complete cytokinesis failure, accounted for only 6.7% and 14.8% of cells in the

two lines, respectively, suggesting that complete cytokinesis failure was relatively uncommon. Nonetheless, we proceeded with quantitative analyses using high-resolution live-cell imaging on these "adapted" lines. Both cyr1cyr2 #1 and #2 lines showed a delay in mitotic progression compared to the control (Figure 2E). Although frameshift mutants could form a bipolar spindle, spindle proportions were distorted. The average spindle width in cyr1cyr2 #1 and cyr1cyr2 #2 frameshift lines was 16.03  $\mu$ m  $\pm$  0.43 and 12.07  $\mu$ m  $\pm$  0.43, respectively, while in control GH line average spindle width was 8.28  $\mu$ m  $\pm$  0.27. On the other hand, spindle length did not change significantly (GH 13.57  $\mu$ m  $\pm$  0.37, cyr1cyr2 #1 13.60  $\mu m \pm 0.47$ ,  $cyr1cyr2 \# 2 \ 12.66 \ \mu m \pm 0.38$ ) (Figure 2F). Phragmoplasts were narrower in frameshift mutants at 8.66  $\mu$ m  $\pm$  0.39 in *cyr1cyr2* #1 and 7.92  $\mu$ m  $\pm$  0.53, in cyr1cyr2 #2, compared to the control 11.32  $\mu m \pm 0.18$  (Figure 2G). To verify the phenotype of the frameshift mutants, we ectopically expressed CYR1-Cerulean under the pEF1 $\alpha$ promoter (Aoyama et al., 2012) in the cyr1cyr2 #2 background. Although the phenotype was not completely restored to wild type, CYR1-Cerulean showed a trend toward rescue in our quantifications (Figures 2D-G). For example, the average spindle width in the CYR1-Cerulean line was reduced to 10.28  $\mu m \pm 0.29$ and the average phragmoplast increased to 9.22  $\mu m$   $\pm$  0.38. We speculate that the incomplete rescue might be due to differences in expression levels between the original gene and the ectopically expressed rescue construct. It is also possible that, since the frameshift line has evolved over time, other adaptive mechanisms may affect cell division phenotypes.

We have also occasionally observed abnormal phragmoplast formation, such as a disorganized phragmoplast or multiple phragmoplasts forming in the "adapted" frameshift lines. This phenotype was observed in 2 out of 11 cells in *cyr1cyr2 #1* and in 4 out of 12 cells in the *cyr1cyr2 #2* line (Supplementary Video 2).

To further assess the potential redundancy between *CYR1* and *CYR2*, we also examined the phenotype of single frameshift mutants, generated using the same gRNAs (Supplementary Figure 2A). In contrast to the double mutants, neither *cyr1* nor *cyr2* single mutants displayed strong growth defects, although quantitative analysis showed that *cyr 1 #30* colonies were slightly smaller comparing to GH (Supplementary Figure 2B, C). Closer investigation of cell division by live-cell imaging did not find any abnormalities in *cyr1* and *cyr2* single mutants (Supplementary Figures 2D–G). These findings support the interpretation that CYR1 and CYR2 have redundant roles in cell division.

We next aimed to visualize the localization of CYR1 and CYR2 in living cells of the wild-type. In *P. patens*, the high rate of homologous recombination enables the creation of endogenously tagged lines, where the tagged protein replaces the native protein (Mueller et al., 2014; Lüth et al., 2023). To visualize the cellular localization of the CYR proteins, we attempted endogenous gene tagging using the mScarlet fluorophore. Although we successfully isolated and verified the tagged lines through genotyping PCR, we were unable to detect fluorescent signals, even with high laser power and extended exposure times. This suggests that CYR proteins are weakly expressed under normal conditions. Next, we constructed vectors for ectopic expression of CYR1 or CYR2 fused to Citrine under the



Frameshift mutations in the cytokinesis-related gene family produce various abnormalities during cell division in protonema cells in *P. patens*. (A) Representative images of moss colonies after 4 weeks of culture: GH is a control, cyr1cyr2 #1 and #2 are independent, adapted frameshift lines (phenotypes weakened over time) isolated through CRISPR genetic screening. Scale, 10 mm. (B) Colony size measured after 4 weeks of culture. Each data point corresponds to a single colony (mean  $\pm$  SEM, \*\*\*\* $p \le 0.0001$  by one-way ANOVA with Dunnett's multiple comparison test against GH) (C) Phylogenetic reconstruction of the CYR gene family based on maximum-likelihood tree inference with midpoint-rooting. Values at internal nodes indicate percentage support by 1000 bootstrap samples. (D) Representative images of cell division in GH, cyr1cyr2 #1, cyr1cyr2#2 and CYR1-Cerulean (rescue line in the cyr1cyr2#2 background). Time zero is set at NEBD, and single focal plane images are shown. Scale, 10  $\mu$  Mitotic duration calculated from NEBD to anaphase onset. Each data point corresponds to a single cell (mean  $\pm$  SEM, \*\*p = 0.041 by one-way ANOVA with Dunnett's multiple comparison test against GH) (F) Spindle dimensions: spindle width (light gray bars) and spindle length (dark gray bars). Each data point corresponds to a single cell (mean  $\pm$  SEM, \*\*\*p = 0.064 by one way ANOVA with Dunnett's multiple comparison test against GH). No statistically significant difference in spindle length found. (G) Phragmoplast length in GH, cyr1cyr2 #1, cyr1cyr2 and CYR1-Cerulean (rescue line in the cyr1cyr2#2 background). Each data point corresponds to a single cell (mean  $\pm$  SEM, \*\*p = 0.0064 by one-way ANOVA with Dunnett's multiple comparison test against GH).

control of the rice actin promoter, which enabled us to observe the localization of these proteins. Both CYR1-Citrine and CYR2-Citrine exhibited cytoplasmic localization prior to nuclear envelope breakdown (NEBD). During cytokinesis, both CYR1 and CYR2 showed bright signals at the phragmoplast midzone and weaker signals throughout the rest of the phragmoplast. These signals expanded as the phragmoplast grew, ultimately fusing with the cell boundaries (Figures 3A, B; Supplementary Video 3). Interestingly, we also occasionally observed multiple phragmoplast formation in the CYR1-Citrine (n=2 out of 7), but not in the CYR2-Citrine overexpression line (n=7) (Supplementary Video 2). While the mechanism remains unclear, no cytokinesis failure or growth defects were detected in these lines.

Taken together, the combination of the cellular phenotype observed after frameshift mutations and the cellular localization data suggests that the CYR gene family function is related to cytokinesis in Physcomitrella. However, the specific role of these genes and their interacting partners remain to be identified.

## Lagging Chromosome (LACH) gene family is essential

Another gene family, named Lagging Chromosome (*LACH*) after the later discovered cellular phenotype, was originally recognized in our CRISPR screening as an essential gene candidate. During CRISPR screening we were able to isolate several non-frameshift mutants, but not plants containing frameshift mutations, suggesting that frameshift mutations in the *LACH* gene family are lethal in *P. patens*. We found the *LACH* gene to be co-expressed with mitotic kinases Haspin (Pp3c5\_21110) and MPS1 (Pp3c6\_320) (Supplementary Table 1). In addition to the *LACH* gene in Physcomitrella (version 3.3: Pp3c25\_4280; version 6.1: Pp6c25\_7230), phylogenetic reconstruction within our species set revealed potential homologs of this gene in other bryophytes, the clubmoss *Diphasiastrum complanatum* and the gymnosperm *Picea abies* (Figure 4A). Protein functionality could not be clearly predicted and no family assignment was inferred by alignment

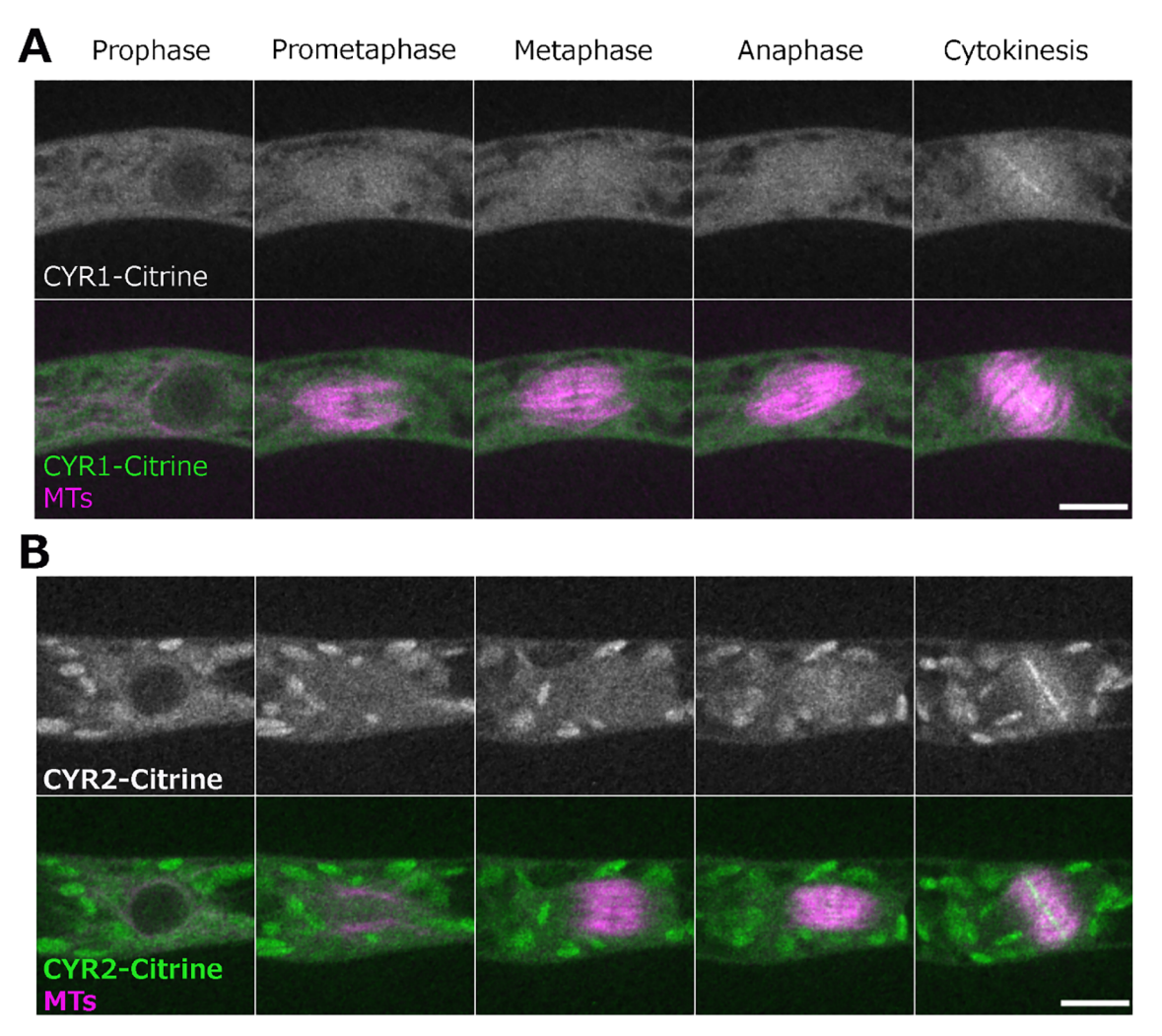


FIGURE 3

Localization of CYR1 and CYR2 during cell division. Live imaging of wild-type *P. patens* caulonemal apical cells expressing mCherry-tubulin (magenta) and (A) CYR1-Citrine (green) or (B) CYR2-Citrine (green). CYR1-Citrine and CYR2-Citrine are ectopically expressed under a rice actin promoter. Images were acquired every 2 min as a Z-stack (5 µm in 2.5 µm steps); best focal plane is shown. Scale, 10 µm.

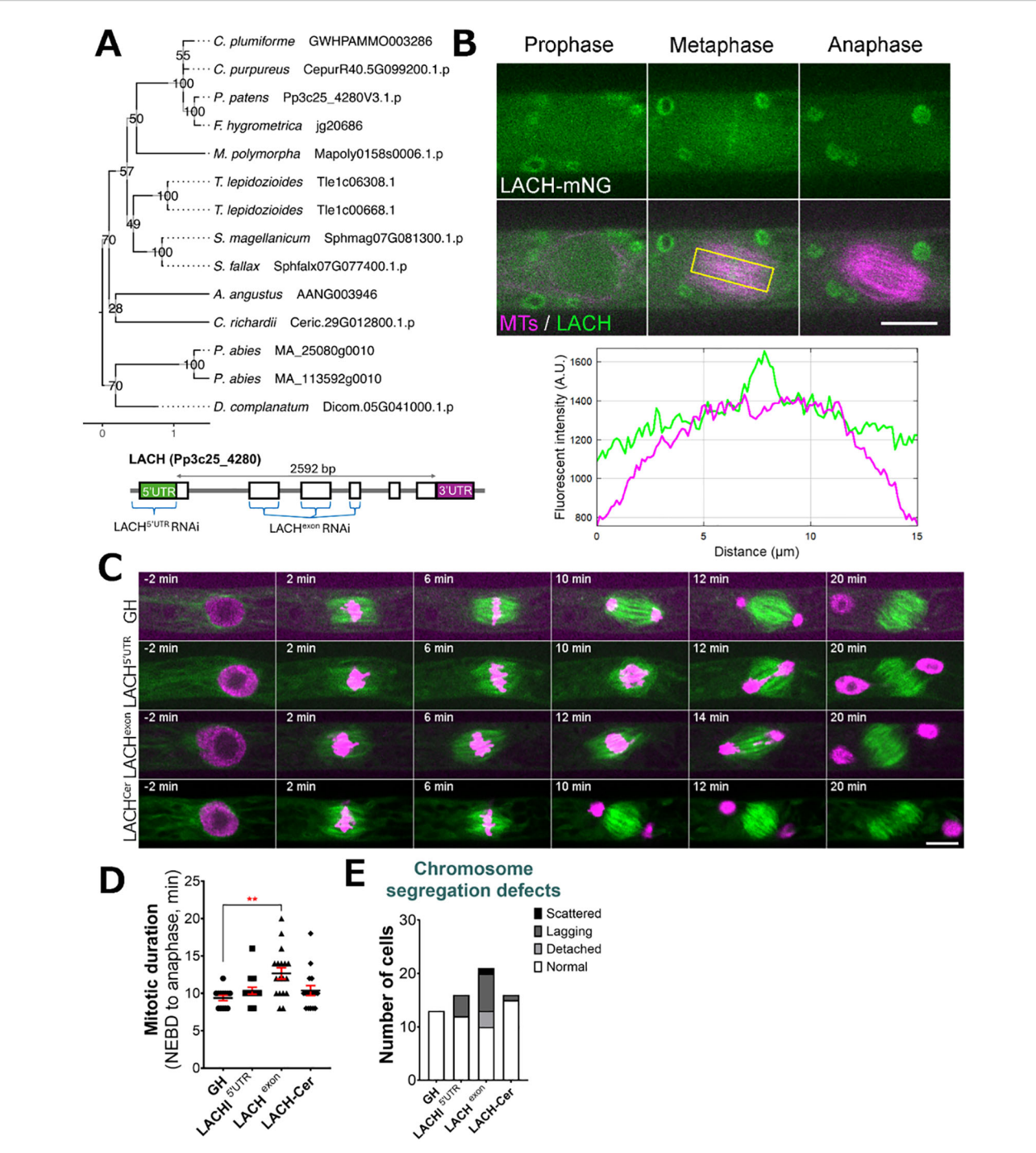


FIGURE 4
LACH localization and phenotype after RNAi knock-down. (A) (top) Phylogenetic reconstruction of the LACH family based on maximum-likelihood tree inference with midpoint-rooting. Values at internal nodes indicate percentage support by 1000 bootstrap samples. (bottom) Gene model of the LACH gene and sites targeted by RNAi. (B) Live imaging of *P. patens* protonemal apical cells expressing mCherry-tubulin (magenta) and LACH-mNeonGreen (green). Plot shows fluorescent intensity distribution (A.U.) in metaphase cell; measured area is indicated with a yellow rectangle. Full localization data can be found in Supplementary Figure 3. Scale, 10 μm. (C) Representative mitotic progression and chromosome missegregation in the LACH RNAi lines. 'GH' is the control line, LACH<sup>Cer</sup> is a rescue line expressing codon-replaced LACH-Cerulean in the LACHexon RNAi background. Scale, 10 μm. (D) Mitotic duration calculated from NEBD to anaphase onset. Each data point corresponds to a single cell (mean ± SEM, \*\*\*p = 0.0008 by one way ANOVA with Dunnett's multiple comparison test against GH) (E) Frequency of chromosome missegregation defects in LACH RNAi lines. Chromosome missegregation defects were classified into three types: chromosomes detached from the metaphase plate (detached chromosomes), lagging chromosomes in anaphase (lagging chromosomes), and scattered (severe chromosome missegregation). Y-axis shows the actual number of cells observed.

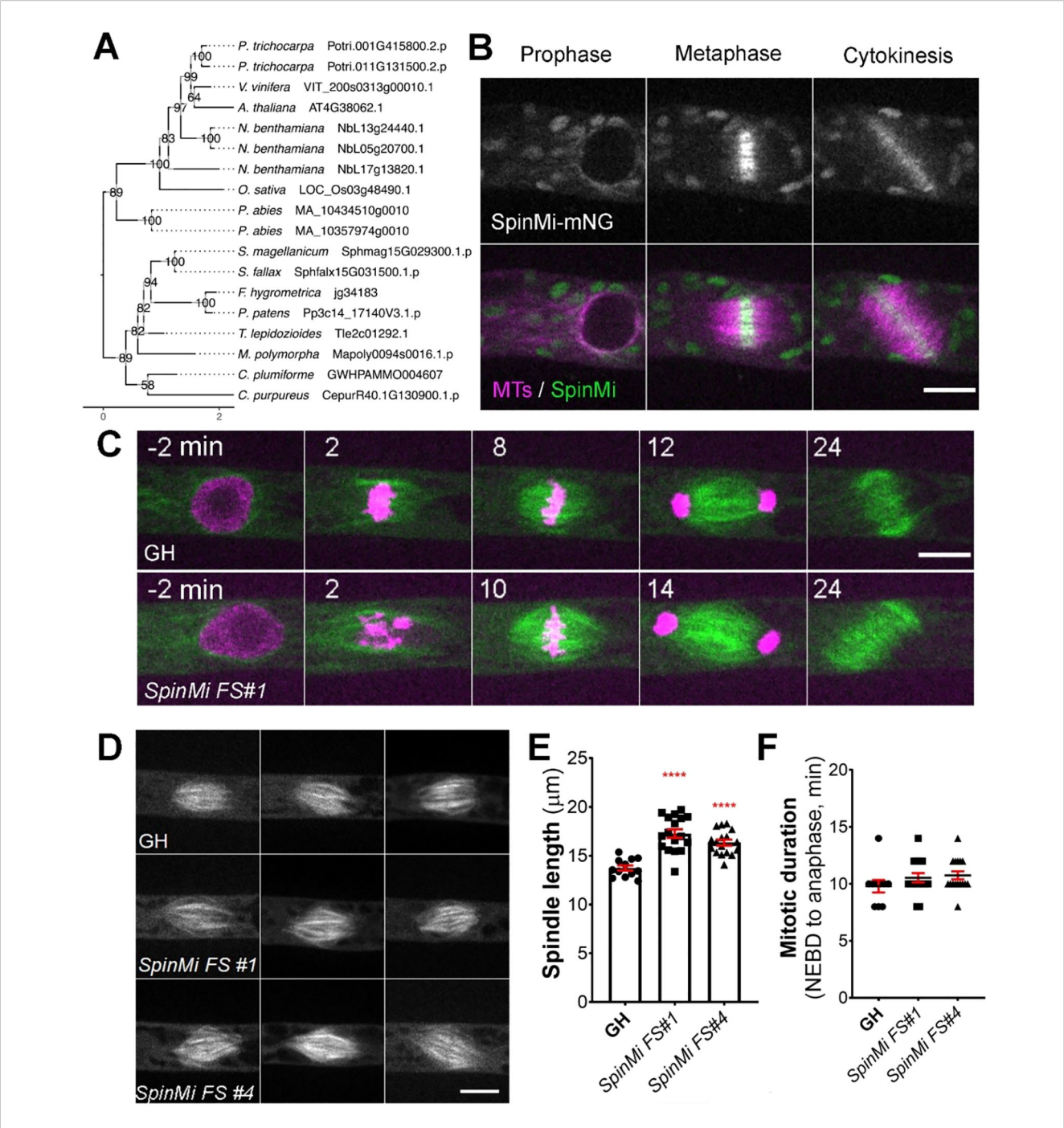


FIGURE 5
SpinMi localization and frameshift phenotype. (A) Phylogenetic reconstruction of the SpinMi family based on maximum-likelihood tree inference with midpoint-rooting. Values at internal nodes indicate percentage support by 1000 bootstrap samples. (B) Live imaging of P. patens protonemal apical cells expressing mCherry-tubulin (magenta) and SpinMi-mNeonGreen (green). Full localization data can be found in Supplementary Figure 3. Scale, 10  $\mu$ m. (C) Representative images of cell division in GH and SpinMi FS#1 (frameshift mutant line). Scale, 10  $\mu$ m. (D) Representative images of metaphase spindles in control (GH), SpinMi FS#1 and SpinMi FS#2 mutant lines. Three spindles per each line are shown. Scale, 10  $\mu$ m. (E) Metaphase spindle length measured in GH, SpinMi FS#1 and SpinMi FS#2. Each data point corresponds to a single cell (mean  $\pm$  SEM, \*\*\*\* $p \le 0.0001$  by one way ANOVA with Dunnett's multiple comparison test against GH) (F) Mitotic duration from NEBD to anaphase onset in GH, SpinMi FS#1 and SpinMi FS#2 lines. No statistically significant difference found. Each data point corresponds to a single cell (mean  $\pm$  SEM).

against the PANTHER database. Our *in-silico* analysis revealed a high probability for localization to the cytoplasm and nucleus (Supplementary Table 2). Since we could not isolate a frameshift line using CRISPR/Cas9, we decided to pursue further

characterization of this gene using different methods. To investigate the localization of LACH protein in living cells, we generated an endogenously tagged line in which the *LACH* gene was fused to the mNeonGreen fluorophore. LACH-mNeonGreen

signals were observed in the cytoplasm and nucleus during interphase. After NEBD, we observed accumulation of brighter signals in the centre of the spindle during prometaphase and metaphase, although overall fluorescent signals intensity was low. These signals disappeared upon the anaphase onset (Figure 4B, Supplementary Figure 3).

Additionally, we aimed to functionally characterize the LACH gene using an inducible RNA interference (RNAi) system, in which RNAi production is triggered by the addition of  $\beta$ -estradiol to the culture medium (Kubo et al., 2013). Since the gene knock-down is triggered only in the presence of β-estradiol, this system is widely used to study essential genes in Physcomitrella (Nakaoka et al., 2012). We designed two independent RNAi constructs: one targeting the 5' UTR region and another targeting an exon region of the LACH gene. After line selection, we observed phenotypic changes following 5-6 days of culture with 1  $\mu$ M  $\beta$ -estradiol in the growth medium, because prolonged culture can complicate data interpretation due to side effects. Overall, we did not notice changes in cell growth or cell shape comparing to the control. A closer investigation of cell division showed that both RNAi constructs led to various chromosome missegregation phenotypes, including detached and/or lagging chromosomes during mitosis (Figure 4C, E). The chromosome missegregation phenotype was more pronounced in the exon RNAi line (Figure 4C, Supplementary Video 4) and similarly, mitotic delay was also more noticeable in the LACH exon RNAi line, which we attribute to the strength of the RNAi line and efficiency of gene knock-down (Figures 4D, E). To confirm the specificity of this phenotype, we generated a rescue line expressing codon-replaced LACH-Cerulean in the background of the exon RNAi construct. This transgene restored normal mitotic timing and significantly reduced the lagging chromosome phenotype, supporting that these defects are due to LACH depletion (Figures 4C-E).

Based on the RNAi phenotype and its localization, we conclude that *LACH* function is related to regulating chromosome segregation during mitosis in *P. patens*.

# SpinMi gene family, identified through localization screening

Besides CRISPR-based genetic screening, we chose 21 gene candidates for additional localization screening. Candidates were selected based on their co-expression with multiple known mitotic genes during the initial gene search (Supplementary Table 1). We speculated that their repeated appearance in our co-expression analysis suggests a higher likelihood that they are involved in cell division.

For the localization screening, we created endogenously tagged versions of these genes by fusing them with the mNeonGreen fluorophore in a background line expressing the microtubule marker mCherry- $\alpha$ -tubulin (Kosetsu et al., 2017). After confirming the correct integration through genotyping PCR, we performed live-cell imaging in protonema cells to observe protein

localization. One of the tagged proteins was distinctly observed at the mitotic spindle and phragmoplast during cell division, prompting us to conduct further analysis. Based on the protein localization, we designated this gene family as *SpinMi* (Spindle and Phragmoplast Midzone).

The *SpinMi* gene family contains a single-copy gene in Physcomitrella (version 3.3: Pp3c14\_17140; version 6.1: Pp6c14\_9440) and appears to be highly conserved across land plants, including vascular plants, with species-specific expansions (Figure 5A). However, similar to the *CYR* and *LACH* gene families, we were unable to detect clear homologs in algae. All identified homologs share an assignment to the PANTHER family OS03G0691500 PROTEIN (PTHR45287) and our *in-silico* predictions revealed hints for localization to the cytoplasm and nucleus (Supplementary Table 2).

During prophase, SpinMi-mNeonGreen was distributed throughout the cytoplasm and was also observed on microtubule bundles that surround the nucleus before NEBD in protonema apical cells (Yin et al., 2025). Following NEBD, SpinMimNeonGreen was observed at the forming mitotic spindle, with a higher fluorescent intensity broadly localized at the spindle midzone. This localization persisted until anaphase, and afterwards SpinMi-mNeonGreen relocated to the forming phragmoplast, with brighter fluorescence observed in the phragmoplast midzone (Figure 5B, Supplementary Figure 4, Supplementary Video 5). To assess whether the localization of SpinMi during mitosis is microtubule-dependent, we treated dividing cells with 20 µM oryzalin, a microtubule-depolymerizing drug (Pressel et al., 2008). Following oryzalin addition, SpinMimNeonGreen signals gradually dissipated following microtubule depolymerization, indicating that SpinMi localization depends on microtubules during cell division (Supplementary Figure 4C).

Next, we sought to investigate the function of SpinMi during mitosis. We isolated two independent frameshift mutants using CRISPR/Cas9 (Supplementary Figure 5A). Upon initial observation, the frameshift mutants appeared to grow normally without any visible defects compared to controls (Supplementary Figures 5B, C). This potentially explains why the *SpinMi* gene was not identified in our CRISPR screening, which focused on targeting moss colonies with noticeable growth defects.

We next examined the cellular phenotype of *spinmi* frameshift mutants during mitosis in protonema cells. Mitotic duration, chromosome segregation, phragmoplast assembly, and cytokinesis all appeared normal in the frameshift mutants (Figures 5C, F). However, upon closer inspection, we observed that the mitotic spindles in *spinmi* frameshift mutants were slightly elongated compared to the control (*SpinMi FS#1* 17.27  $\mu$ m  $\pm$  0.43, *SpinMi FS#2* 16.24  $\mu$ m  $\pm$  0.29 vs GH 13.74  $\mu$ m  $\pm$  0.26) (Figures 5D, E). Despite this, no detrimental effects on cell division were evident under normal conditions. *SpinMi* may contribute to fine-tuning spindle architecture, as suggested by its localization and the observed subtle increase in spindle length in mutant lines.

## Discussion

This study was originally designed as a proof of concept that genetic screening combined with the analysis of co-expression data has the power to identify novel genes associated with specific cellular process, specifically cell division, in the model bryophyte *P. patens*. In the context of cell division, expression profiles from synchronized cell cultures in both animal and plant models are often employed to determine which genes are involved in this process (Menges and Murray, 2002; Bar-Joseph et al., 2008). While this method has its merits, it also presents challenges; for instance, not all plant models have established protocols for cell cycle synchronization, and such treatments might be disruptive, potentially affecting gene expression.

We utilized publicly available co-expression data from the Phytozome database, specifically the JGI Plant Gene Atlas project, which contains comprehensive transcriptome data from various growth conditions, different developmental stages (protonema, gametophore, sporophyte, etc.), and multiple laboratories (Perroud et al., 2018; Sreedasyam et al., 2023). We hypothesized that even without cell synchronization, cell division genes might exhibit coexpression under similar conditions and/or life stages. Among the genes we selected for screening, we identified three novel gene families that are likely associated with cell division in the moss P. patens. To the best of our knowledge, these gene families have not been functionally characterised previously and homology inference did not provide sufficient insights. However, phylogenetic analysis allowed us to trace the ancestry of all three gene families back to early land plants, including liverworts and the moss Takakia, which is sister to all other mosses (Hu et al., 2023). Strikingly, we did not find clear homologs in Streptophyte algae, the closest relatives to land plants (Hess et al., 2022). This raises the question of whether the emergence of the families described in our study is a consequence of the transition to land colonization. Furthermore, the functional roles of these genes remain enigmatic, as predicted functionalities of two of them (CYR and LACH) do not match any well-characterized PANTHER annotations and no functional domain annotation was found. This suggests that their cellular function may involve yet-tobe-understood mechanisms.

Our findings regarding the *CYR* gene family indicate a strong association with cytokinesis in *P. patens*. The cellular localization of CYR1 and CYR2 at the phragmoplast midzone, along with the cytokinesis defects observed in frameshift mutants, suggests that these proteins play a role in phragmoplast microtubule dynamics and/or cell plate formation. While their precise molecular function remains unknown, their localization pattern is reminiscent of secretory carrier membrane proteins (SCAMPs) and kinesin12-II, which drives vesicle transport in the *P. patens* phragmoplast overlapping anti-parallel microtubules in the phragmoplast (Yamada et al., 2025). Unlike kinesin12-II, CYR proteins do not contain known microtubule-binding domains or motor motifs, its annotation as GPI-anchored protein suggests that it may be a membrane-bound protein.

Interestingly, we occasionally observed multiple phragmoplast formations in the CYR1-Citrine overexpression line and cyr1cyr2

frameshift mutants, but not in the CYR2-Citrine line (Supplementary Video 2). It is possible that either overexpression or fluorophore tagging of CYR1, or a combination of these factors, acts in a dominant-negative way and can recapitulate some of the cellular phenotypes observed in the CRISPR frameshift mutants. However, we did not observe cytokinesis failure or growth defects, suggesting that negative effects remain mild.

The incomplete rescue observed in ectopic CYR1-Cerulean expression lines suggests that tight regulation of CYR protein expression levels may be necessary for proper function. Further biochemical and genetic studies will be required to clarify their precise molecular roles.

Our characterization of the LACH gene family suggests a function related to chromosome segregation. CRISPR-induced mutants for LACH contained exclusively in-frame mutations. We did not attempt homology-directed knock-in of a stop codon, but our inability to recover null mutants, combined with RNAi phenotypes, supports a role for LACH in essential mitotic functions. The fact that we were unable to isolate viable LACH frameshift mutants further supports the notion that *LACH* is crucial for the moss, and that its loss is lethal. The localization of LACH protein at the spindle midzone and its loss-of-function phenotype, which includes chromosome missegregation and mitotic delay, strongly suggest an involvement in chromosome cohesion and/or microtubule-kinetochore attachment. During cell division, kinetochore proteins show clear dot-like localization patterns in Physcomitrella (Kozgunova et al., 2019), which was not observed in the LACH-mNeonGreen line. Therefore, we suggest that the LACH protein is not a part of the kinetochore complex. However, it is possible that LACH is indirectly involved in centromere/ kinetochore formation. For example, in Arabidopsis cenH3 histone chaperone NASP does not show a clear centromeric localization, but its reduced expression affects deposition of centromeric histone H3 (Le Goff et al., 2020). Another possibility is that LACH function is related to the cohesin complex, which mediates cohesion between replicated sister chromatids and is essential for chromosome segregation in dividing cells. Cohesin complex role during mitosis have not been investigated in Physcomitrella, however in maize, cohesin subunit Structural Maintenance of Chromosome3 (SMC3) mutants show premature loss of sister chromatid cohesion and chromosomes missegregation (Zhang et al., 2020a). Future research could explore whether LACH functions through direct interactions with cohesion regulators or kinetochores.

The third gene family, *SpinMi*, was not identified through CRISPR screening, but rather through localization analysis. This highlights a limitation of our CRISPR screening approach: genes that do not exhibit a strong phenotype after mutation are less likely to be identified using our workflow, which focuses on colonies with growth defects or candidates for essential genes (as indicated by the absence of frameshift mutations). Conducting a localizome screening can serve as either an alternative to, or a complement for, CRISPR screening. In *P. patens*, SpinMi-mNeonGreen localized to the spindle and phragmoplast midzone in a microtubule-dependent manner. Microtubule polarity in mitosis is typically

oriented with most of microtubules plus-ends directed toward the spindle and phragmoplast midzone (Dhonukshe et al., 2006). Therefore, it is possible that SpinMi preferentially binds to the plus-ends of microtubules or forms a complex with other plus-endbinding proteins. Although spinmi frameshift mutants did not exhibit severe defects in mitotic progression, the subtle increase in spindle length suggests that SpinMi plays a role in fine-tuning microtubule organization during mitosis. For example, elongated spindles have also been observed following the knockdown of microtubule-nucleating proteins such as γ-tubulin and augmin in Physcomitrella and Arabidopsis (Nakaoka et al., 2012; Romeiro Motta et al., 2024). The loss of SpinMi may alter the dynamic properties of microtubules, potentially affecting the balance of forces exerted by motor proteins and microtubule-associated proteins that regulate spindle assembly. Given that SpinMi homologs are highly conserved in land plants, it is also of interest to investigate their functions in other model plants and in meiosis.

Our findings offer insights into the genetic components of cell division in early land plants and provide a workflow that integrates CRISPR-based genetic screening with co-expression analysis for gene discovery in the popular model bryophyte *P. patens*. Compared to traditional forward genetics screening, our approach bypasses the need for large-scale mutagenesis and segregation analysis by targeting high-confidence candidates directly. Although transformation and genotyping are still required, the co-expression-based filtering dramatically reduces the search space. Nonetheless, we acknowledge that genes producing weak or lethal phenotypes are likely to be missed in our workflow.

The identification of three novel gene families, unique to land plants, suggests that their emergence was linked to the evolutionary transition from aquatic to terrestrial environments. This transition likely required significant adaptations to the cell division machinery, in response to the dramatic changes in the environment and the need for complex organ development. Moving forward, future studies can focus on further functional analysis of *CYR*, *LACH* and *SpinMi* gene families, investigating their potential interactions with known mitotic regulators, and exploring their functional conservation across different plant lineages to better understand how they contribute to plant cell division and growth.

## Materials and methods

## P. patens culture and transformation

We used *P. patens* lines derived from the Gransden strain (International Moss Stock Center IMSC, accession number 40001), which were maintained at 25 °C under continuous light conditions. Protoplast transformation was carried out according to Hohe et al. (2004) using protoplasts prepared from protonema tissue after 6–7 days of culture. To isolate protoplasts, the protonemata was incubated in a solution containing 2% driselase and 8% (w/v) mannitol for 30 min at room temperature with gentle rocking. The resulting suspension was filtered through a 50 µm nylon mesh and

centrifuged at 180 × g for 2 min to pellet the protoplasts. After discarding the supernatant, the protoplasts were washed twice with 20 mL of 8% mannitol. Prior to transformation, the protoplast concentration was adjusted to  $1.6 \times 10^6$  cells per mL using MMM solution (0.1% MES, pH 5.6, 15 mM MgCl<sub>2</sub>, and 9.1% (w/v) mannitol). Next, 300 µL of the prepared protoplasts were combined with 30  $\mu L$  of plasmid DNA (30  $\mu g$ ) and 300  $\mu L$  of 40% (w/v) polyethylene glycol solution (10 mM Tris-HCl, pH 8.0, 100 mM Ca (NO<sub>3</sub>)<sub>2</sub>, and 8% mannitol). For gRNA transformation, equal amounts of circular gRNA plasmid and Streptococcus pyogenes Cas9 expression vector were simultaneously transferred into the moss. The mixture was incubated at 45 °C for 5 min, followed by 10 min at 20 °C, and subsequently maintained overnight at 25 °C in darkness. The transformed protoplasts were then plated on protoplast regeneration medium plates overlaid with sterile cellophane. After three days of growth, the regenerated protoplasts were transferred onto BCDAT medium containing the appropriate antibiotics for selection (Hohe et al., 2004; Yamada et al., 2016). Genomic integration of transgenes was verified through genotyping PCR and/or sequencing for CRISPR-edited lines. For transformation experiments, the GH line, which expresses histone H2B-mRFP and GFP-α-tubulin, was utilized for CRISPR and RNAi studies (Nakaoka et al., 2012). The line expressing mCherry- $\alpha$ -tubulin under  $EF1\alpha$ promoter was used as a background line for Citrine and mNeonGreen tagging experiments (Kosetsu et al., 2017). A complete list of the transgenic lines generated in this study is provided in Supplementary Table 3.

For colony growth assays, protoplasts were prepared from moss protonemata using driselase treatment and mannitol wash, following the same protocol as used for gene transformation. Following 2–3 weeks of protoplast regeneration, individual colonies were selected and transferred to standard BCDAT agar plates for further growth. Since each colony is presumed to originate from a single protoplast, this approach ensures that differences in colony size reflect growth phenotypes rather than variations in the initial amount of starting tissue.

## Gene selection for screening

We utilized publicly available transcriptome data from the Joint Genome Institute (JGI) Gene Atlas Project (http://jgi.doe.gov/doe-jgi-plant-flagship-gene-atlas/), based on P. patens genome annotation version 3.3 (Lang et al., 2018) and accessed via Phytozome (https://phytozome-next.jgi.doe.gov/) (Perroud et al., 2018). A list of known mitotic genes in P. patens was compiled based on previous functional studies. This list was not exhaustive but served as a test for our workflow (Supplementary Table 1). For each mitotic gene, we manually examined co-expression networks and selected genes with a co-expression score of  $\geq$ 0.8 (arbitrarily chosen). We further refined this list by excluding genes with previously reported functions (verified through P. patens and A. thaliana homolog searches) and those with clearly defined nonmitotic roles based on PANTHER annotations (e.g., metabolic

enzymes). The final selection of genes is provided in Supplementary Table 1.

# *In silico* prediction of protein function and localization

We mapped gene models from the *P. patens* annotation version 3.3 (Lang et al., 2018) to the most recent version 6.1 (Bi et al., 2024) and found no changes on CDS and thus amino acid level. Annotation of functional domains and possible family associations for our candidate sequences was inferred with InterProScan (version 5.71-102.0; (Jones et al., 2014)). We then used DeepLoc (version 2.1; (Ødum et al., 2024)), LOCALIZER (version 1.0.4; (Sperschneider et al., 2017)), TargetP (version 2.0; (Armenteros et al., 2019)) and SignalP (version 6.0; (Teufel et al., 2022)) to predict subcellular localization.

# gRNA library construction and molecular cloning

CRISPR gRNAs were designed using the online tool CRISPOR (http://crispor.tefor.net/), based on target gene specificity (off-target score) and predicted frameshift efficiency (Concordet and Haeussler, 2018). The target site was selected within an exon common to all transcript variants per Phytozome data. When multiple homologs were present, we prioritized designing a single gRNA targeting a conserved site. gRNAs were synthesized as single-stranded primers, which also contained overhangs, matching the BsaI-generated overhangs in the destination vector. Forward and reverse primers for each gRNA were mixed together and annealed in the PCR thermocycler. Next, generated individual gRNAs were ligated into pCasGuide/pUC18 vector pre-digested with BsaI, between the U6 promoter and gRNA scaffold sequence (Collonnier et al., 2017). The destination vector for gRNA also contained a hygromycin resistance cassette for plant selection. Each plasmid in the gRNA library was verified by sequencing to confirm correct integration of the gRNA. In case when three or more gRNA were required to target all homologs in the respective gene family, we carried out an additional cloning step to assemble all gRNAs into a single vector (Leong et al., 2018). In this case, individual gRNAs together with the U6 promoter and gRNA scaffold region were amplified by PCR and assembled into a single multi-gRNA plasmid using an in-house Gibson assembly mix (Gibson et al., 2009).

Plasmids for mNeon-Green endogenous tagging were also assembled using Gibson assembly, with mNeonGreen gene and antibiotic resistance cassette flanked by homologous recombination regions (500–800 bp of the respective genes). A detailed protocol for endogenous gene tagging and knockouts in *P. patens* has been published previously (Yamada et al., 2016). RNAi vectors were

cloned using the Gateway system (Invitrogen, Carlsbad, CA, USA), with pGG624 as the destination vector (Miki et al., 2016). Two independent, non-overlapping RNAi constructs were prepared for each gene. The full list of plasmids and primers used in this study is shown in Supplementary Table 3, except for gRNA library primers and plasmids which are shown in Supplementary Table 1.

## Microscopy and data analysis

For most samples we used agar-coated glass-bottom dishes for moss culture. A small piece of moss protonema was placed on top of the BCD agar medium and cultured under continuous light at 25 °C for 4-5 days prior to observation (Yamada et al., 2016). For RNAi induction,  $\beta$ -estradiol was added to BCD agar medium at a final concentration of 1 µM (Nakaoka et al., 2012). Oryzalin was diluted in 1 mL of distilled water to a final concentration of 20  $\mu M$ and added directly to the sample during live-cell imaging. For the cyr1cyr2 frameshift line, due to strong growth defects, we used a microfluidic device to acquire enough data for quantification (Bascom et al., 2016). The PDMS device mold was prepared by spin-coating negative photoresist (SU-8 3025) on a silicon wafer, and microchannel designs were created using a maskless lithography system (DL-1000). The PDMS pre-polymer mixture (Sylgard 184) was prepared by mixing the elastomer base and curing agent at a 10:1 ratio, poured onto the mold, degassed for 30 min, and cured in an oven at 65 °C for 90 min. The microchannel inlet was punched using a 1.5-mm biopsy punch. The PDMS device and glass-bottom dish were treated with air plasma for 30 seconds, pressed together, and heated at 65 °C for 2 h to achieve irreversible bonding. To introduce moss cells in the device, we collected a small piece of protonema grown on cellophane after 5-7 days of culture and blended it in 5 mL BCDAT liquid medium. The suspension was injected into the microdevice. To prevent evaporation, the device was submerged in BCDAT medium, sealed with parafilm, and incubated at 25 °C under continuous light for 3-4 days (Kozgunova and Goshima, 2019; Yoshida and Kozgunova, 2023).

Most images were acquired using a Nikon Ti microscope  $(60 \times 1.30\text{-NA} \text{ lens}; \text{Nikon}, \text{Tokyo}, \text{Japan})$  equipped with a CSU-X1 spinning-disk confocal unit (Yokogawa, Tokyo, Japan) and an electron-multiplying charge-coupled device camera (ImagEM; Hamamatsu, Hamamatsu, Japan). The microscope was controlled using the NIS-Elements software (Nikon). Imaging after FM4–64 staining and original observation of *cyr1cyr2* frameshift lines (Supplementary Figure 1B, Supplementary Video 1) were performed using a ZEISS inverted microscope  $(25 \times 0.8\text{-NA} \text{ lens} \text{ or } 63 \times 1.4\text{-NA} \text{ lens}, \text{Carl Zeiss Microscopy}, Germany)$  equipped with a CSU-X1 spinning-disk confocal unit (Yokogawa, Tokyo, Japan) and CCD camera (Photometrics Prime sCMOS). All imaging was performed at 22–24 °C in the dark. Imaging was performed at least twice for localization and at

least three times for phenotypic characterization. To obtain quantitative values, the data from multiple experiments were combined because of insufficient sample numbers in a single experiment. Moss colony images were acquired after 4 weeks of culture using a smartphone camera. Image data were analyzed using ImageJ (National Institutes of Health, Bethesda, MD, USA). Prism was used for the graphs and statistical analyses (GraphPad, San Diego, CA, USA).

# Homolog identification and phylogenetic reconstruction

Based on the Physcomitrella reference sequences identified in this study, we conducted proteome-wide sequence searches with blastp (version 2.16.0+; (Altschul et al., 1997)) against Anthoceros angustus (Zhang et al., 2020b), Arabidopsis thaliana (Cheng et al., 2017), Calohypnum plumiforme (Mao et al., 2020), Ceratodon purpureus (Carey et al., 2021), Ceratopteris richardii (Marchant et al., 2022), Chara braunii (Nishiyama et al., 2018), Chlamydomonas reinhardtii (Merchant et al., 2007), Chlorella sp (Hamada et al., 2018), Cyanophora paradoxa (Price et al., 2019), Diphasiastrum complanatum (v3.1, DOE-JGI, http://phytozome-next.jgi.doe.gov), Dunaliella salina (Polle et al., 2017), Funaria hygrometrica (Kirbis et al., 2025), Galdieria sulphuraria (Rossoni et al., 2019), Klebsormidium nitens (Hori et al., 2014), Marchantia polymorpha (Bowman et al., 2017), Mesotaenium endlicherianum (Cheng et al., 2019), Microglena sp (Ye et al., 2022), Nicotiana benthamiana (Ranawaka et al., 2023), Oryza sativa (Ouyang et al., 2007), Picea abies (Nystedt et al., 2013), Populus trichocarpa (Tuskan et al., 2006), Selaginella moellendorffii (Banks et al., 2011), Sphagnum fallax (Healey et al., 2023), Sphagnum magellanicum (Healey et al., 2023), Spirogloea muscicola (Cheng et al., 2019), Takakia lepidozioides (Hu et al., 2023), Vitis vinifera (Jaillon et al., 2007) and Volvox carteri (Prochnik et al., 2010). To filter out nonhomologous sequences, initial blast hits were manually curated, functional annotation was inferred with InterProScan (version 5.71-102.0; (Jones et al., 2014)) and several iterations of multiple sequence alignments and maximum-likelihood tree inferences were performed with MAFFT (version 7.525; (Katoh and Standley, 2013)) and FastTree (version 2.1.11; (Price et al., 2010)). During the final round, best-fit models were identified with ModelTest-NG (Darriba et al., 2020) and maximum likelihood trees were calculated with RAxML-NG (Kozlov et al., 2019) using the 'JTT+I+G4' (LACH) and 'JTT+I+G4+F' (CYR, SpinMi) models and 1000 bootstrap replicates. Final trees were midpoint-rooted and visualized using R (version 4.3.3, R Core Team, 2024) and the ggtree package (version 3.10.1 (Yu et al., 2017)).

## Data availability statement

The sequencing data presented in the study are deposited in the GenBank repository, accession numbers PX549057-PX549065.

## **Author contributions**

KM: Investigation, Validation, Visualization, Writing – original draft, Writing – review & editing. NvG: Formal analysis, Investigation, Methodology, Validation, Visualization, Writing – original draft, Writing – review & editing. RR: Conceptualization, Funding acquisition, Supervision, Writing – original draft, Writing – review & editing. EK: Conceptualization, Data curation, Formal analysis, Funding acquisition, Investigation, Methodology, Project administration, Resources, Software, Supervision, Validation, Visualization, Writing – original draft, Writing – review & editing.

## **Funding**

The author(s) declare financial support was received for the research and/or publication of this article. This work was funded by Japan Society for the Promotion of Science (KAKENHI) 23K14210 and Research Grant for Young Japanese Researchers from the Nakajima Foundation to EK, German Research Foundation DFG under Germany's Excellence Strategy (CIBSS – EXC-2189 – Project ID 390939984) to RR.

## Acknowledgments

We would like to thank Dr. Moé Yamada for comments on the manuscript, and the Life Imaging Center at the University of Freiburg for microscopic use. We are grateful for the support by the High Performance and Cloud Computing Group at the Zentrum für Datenverarbeitung of the University of Tübingen, the state of Baden-Württemberg through bwHPC and the German Research Foundation DFG through grant INST 37/935–1 FUGG, as well as the de.NBI Cloud within the German Network for Bioinformatics Infrastructure (de.NBI), ELIXIR-DE (Forschungszentrum Jülich and W-de.NBI-001, W-de.NBI-004, W-de.NBI-008, W-de.NBI-010, W-de.NBI-013, W-de.NBI-014, W-de.NBI-016, W-de.NBI-022). Open Access Funding was enabled and organized by Projekt DEAL.

## Conflict of interest

The authors declare that the research was conducted in the absence of any commercial or financial relationships that could be construed as a potential conflict of interest.

## Generative AI statement

The author(s) declare that no Generative AI was used in the creation of this manuscript.

Any alternative text (alt text) provided alongside figures in this article has been generated by Frontiers with the support of artificial intelligence and reasonable efforts have been made to ensure

accuracy, including review by the authors wherever possible. If you identify any issues, please contact us.

## Publisher's note

All claims expressed in this article are solely those of the authors and do not necessarily represent those of their affiliated organizations, or those of the publisher, the editors and the reviewers. Any product that may be evaluated in this article, or claim that may be made by its manufacturer, is not guaranteed or endorsed by the publisher.

## Supplementary material

The Supplementary Material for this article can be found online at: https://www.frontiersin.org/articles/10.3389/fpls.2025.1653765/full#supplementary-material

#### SUPPLEMENTARY FIGURE 1

Frameshift verification and initial phenotype observation in cyr1cyr2#1 and #2 frameshift lines. (A) Gene models for cyr1 and cyr2 genes, and frameshift mutations confirmed by sequencing in cyr1cyr2#1 and cyr1cyr2#2 moss lines. The gRNA target site is indicated with a blue box. (B) Membrane staining with 10  $\mu$ M of lipophilic dye FM4-64. Nucleus and membranes in same color. Cyan arrowheads point to nuclei, red arrowheads point to cell walls. Note binucleated cell ( $2^{nd}$  panel), multiple cell walls ( $3^{rd}$  panel), and incomplete cell wall ( $4^{th}$  panel) in the cyr1cyr2#2 mutant. Scale, 10  $\mu$ m. (C) Membrane staining in the adapted cyr1cyr2#1 and cyr1cyr2#2 lines after repeated culture. Cyan arrowheads point to multinuclei, red arrowheads point to defective cell walls, yellow arrowheads point to abnormal branching. Scale, 50  $\mu$ m. (D) Number of cells with different phenotypes observed in the adapted cyr1cyr2#1 and cyr1cyr2#2 lines.

#### SUPPLEMENTARY FIGURE 2

Frameshift verification and phenotype observation in cyr1 and cyr2 single frameshift lines. (A) Gene models for cyr1 and cyr2 genes, and frameshift mutations confirmed by sequencing in cyr1#30 and cyr2#1 and #4 lines. The gRNA target site is indicated with a blue box. (B) Representative images of moss colonies after3 weeks of culture. Scale, 10 mm. (C) Colony size measured after 3 weeks of culture. Each data point corresponds to a single colony (mean  $\pm$  SEM, \*\*p=0.0089, \*p=0.04 by one-way ANOVA with Dunnett's multiple comparison test against GH) (D) Representative images of cell division in GH, cyr1 FS #30, and cyr2 FS #4. Time zero is set at NEBD, and single focal plane images are shown. Scale, 10  $\mu m$ . (E) Mitotic duration calculated from NEBD to anaphase onset. Each data point corresponds to a single cell (F) Spindle dimensions: spindle width (light gray bars) and spindle length (dark gray bars). Each data point corresponds to a single cell (G) Phragmoplast length in GH, cyr1 FS #30, and cyr2 FS #4. Each data point corresponds to a single cell. No statistically significant difference was found in cyr1 FS #30, and cyr2 FS #4 (G-F) against control (G, H)

#### SUPPLEMENTARY FIGURE 3

Localization of LACH-mNeonGreen during mitosis. (A) Live imaging of mitosis in caulonemal apical cells, expressing mCherry-tubulin as a microtubule marker (magenta). AF panel shows cell autofluorescence background, including chloroplast autofluorescence. Scale, 10  $\mu m$ . (B) Live imaging of P. patens protonemal apical cells expressing mCherry-tubulin (magenta) and LACH-mNeonGreen (green). Scale, 10  $\mu m$ .

#### SLIDDI EMENITADY EIGLIDE A

Localization of SpinMi during cell division. Live imaging of *P. patens* caulonemal apical cells expressing **(A)** mCherry-tubulin and **(B)** mCherry-tubulin and SpinMi-mNeonGreen. AF panel shows cell autofluorescence background, including chloroplast autofluorescence. **(C)** Microtubule-depolymerizing drug oryzalin, at final concentration 20 µM, was added during prometaphase to the cell expressing mCherry-tubulin/SpinMi-mNeonGreen. Scale, 10 µm.

#### SUPPLEMENTARY FIGURE 5

Frameshift mutations in SpinMi do not cause serious growth defects. (A) Gene model of SpinMi and confirmation of frameshift mutations in the SpinMi gene by sequencing. The gRNA target site is indicated with a blue box. (B) Representative images of GH, SpinMi FS#1 and SpinMi FS#2 colonies after one month culture. (C) Colony size after one month of culture. No statistically significant difference found with one way ANOVA with Dunnett's multiple comparison test against GH. Each data point corresponds to a single colony (mean + SEM).

#### SUPPLEMENTARY VIDEO 1

Cytokinesis failure was observed in cyr1cyr2 #1 and #2 CRISPR lines. Live-cell imaging was performed in *P. patens* apical caulonemal cells in cyr1cyr2 #1 and cyr1cyr2 #2 CRISPR frameshift line expressing GFP-tubulin (green) and H2B-RFP (magenta). Images were acquired every 2 min in a single focal plane. Scale, 10  $\mu$ m.

#### SUPPLEMENTARY VIDEO 2

Multiple phragmoplast formation cyr1cyr2 #2 CRISPR line and CYR1-Citrine overexpression line. Live-cell imaging was performed in P. patens apical caulonemal cells in cyr1cyr2 #2 CRISPR frameshift line, expressing GFP-tubulin (left panel, green) and H2B-RFP (left panel, magenta), and CYR1-Citrine (right panel, green) overexpression line, which also expressed mCherry-tubulin (magenta, right panel) as a microtubule marker. Secondary phragmoplast formation is indicated with white arrows. Images were acquired every 2 min as a Z-stack (5  $\mu$ m in 2.5  $\mu$ m steps), best focal plane is shown. Scale, 10  $\mu$ m.

#### SUPPLEMENTARY VIDEO 3

Localization of CYR1-Citrine and CYR2-Citrine. Live-cell imaging was performed in P. patens apical caulonemal cells expressing mCherry-tubulin (magenta) and one of the following tagged proteins (green): CYR1-Citrine, CYR2-Citrine or Citrine. Images were acquired every 2 min as a Z-stack (5  $\mu$ m in 2.5  $\mu$ m steps), best focal plane is shown. Scale, 10  $\mu$ m.

#### SUPPLEMENTARY VIDEO 4

Chromosome missegregation after inducible RNAi knockdown of LACH. Representative images of mitotic progression and chromosome missegregation caused by depletion of LACH. RNAi was induced by addition of  $\beta$ -estradiol to the growth medium at final concentration of 1  $\mu\text{M}, 5-6$  days prior to observation. Images were acquired every 2 min as a Z-stack (5  $\mu\text{m}$  in 2.5  $\mu\text{m}$  steps); best focal plane is shown. Scale, 10  $\mu\text{m}$ .

#### SUPPLEMENTARY VIDEO 5

Localization of SpinMi-mNeonGreen. Live-cell imaging was performed in P. patens apical caulonemal cells expressing mCherry-tubulin (magenta) and SpinMi-mNeonGreen (green). Images were acquired every 2 min as a Z-stack (5  $\mu$ m in 2.5  $\mu$ m steps), best focal plane is shown. Scale, 10  $\mu$ m.

#### SUPPLEMENTARY TABLE 1

Genes and gRNA library used for CRISPR genetic screening.

#### SUPPLEMENTARY TABLE 2

Results of  $in\ silico$  prediction of subcellular localization

#### SUPPLEMENTARY TABLE 3

P. patens transgenic lines, primers, and vectors used in this study

## References

Altschul, S. F., Madden, T. L., Schäffer, A. A., Zhang, J., Zhang, Z., Miller, W., et al. (1997). Gapped BLAST and PSI-BLAST: a new generation of protein database search programs. *Nucleic Acids Res.* 25, 3389–3402. doi: 10.1093/nar/25.17.3389

Aoyama, T., Hiwatashi, Y., Shigyo, M., Kofuji, R., Kubo, M., Ito, M., et al. (2012). AP2-type transcription factors determine stem cell identity in the moss *Physcomitrella patens*. *Development* 139, 3120–3129. doi: 10.1242/dev.076091

Armenteros, J. J. A., Salvatore, M., Emanuelsson, O., Winther, O., Von Heijne, G., Elofsson, A., et al. (2019). Detecting sequence signals in targeting peptides using deep learning. *Life Sci. Alliance* 2, e201900429. doi: 10.26508/lsa.201900429

Banks, J. A., Nishiyama, T., Hasebe, M., Bowman, J. L., Gribskov, M., DePamphilis, C., et al. (2011). The selaginella genome identifies genetic changes associated with the evolution of vascular plants. *Science* 332, 960–963. doi: 10.1126/science.1203810

Bar-Joseph, Z., Siegfried, Z., Brandeis, M., Brors, B., Lu, Y., Eils, R., et al. (2008). Genome-wide transcriptional analysis of the human cell cycle identifies genes differentially regulated in normal and cancer cells. *Proc. Natl. Acad. Sci. U.S.A.* 105, 955–960. doi: 10.1073/pnas.0704723105

Bascom, C. S., Wu, S.-Z., Nelson, K., Oakey, J., and Bezanilla, M. (2016). Long-term growth of moss in microfluidic devices enables subcellular studies in development. *Plant Physiol.* 172, 28–37. doi: 10.1104/pp.16.00879

Bi, G., Zhao, S., Yao, J., Wang, H., Zhao, M., Sun, Y., et al. (2024). Near telomere-to-telomere genome of the model plant *Physcomitrium patens*. *Nat. Plants* 10, 327–343. doi: 10.1038/s41477-023-01614-7

Bowman, J. L., Kohchi, T., Yamato, K. T., Jenkins, J., Shu, S., Ishizaki, K., et al. (2017). Insights into Land Plant Evolution Garnered from the *Marchantia polymorpha* Genome. *Cell* 171, 287–304.e15. doi: 10.1016/j.cell.2017.09.030

Buschmann, H., and Zachgo, S. (2016). The evolution of cell division: from streptophyte algae to land plants. *Trends Plant Sci.* 21, 872–883. doi: 10.1016/j.tplants.2016.07.004

Camilleri, C., Azimzadeh, J., Pastuglia, M., Bellini, C., Grandjean, O., and Bouchez, D. (2002). The arabidopsis *TONNEAU* 2 gene encodes a putative novel protein phosphatase 2A regulatory subunit essential for the control of the cortical cytoskeleton. *Plant Cell* 14, 833–845. doi: 10.1105/tpc.010402

Carey, S. B., Jenkins, J., Lovell, J. T., Maumus, F., Sreedasyam, A., Payton, A. C., et al. (2021). Gene-rich UV sex chromosomes harbor conserved regulators of sexual development. *Sci. Adv. 7*, eabh2488. doi: 10.1126/sciadv.abh2488

Chater, C. C., Caine, R. S., Tomek, M., Wallace, S., Kamisugi, Y., Cuming, A. C., et al. (2016). Origin and function of stomata in the moss *Physcomitrella patens*. *Nat. Plants* 2, 16179. doi: 10.1038/nplants.2016.179

Cheng, C. Y., Krishnakumar, V., Chan, A. P., Thibaud-Nissen, F., Schobel, S., and Town, C. D. (2017). Araport11: a complete reannotation of the *Arabidopsis thaliana* reference genome. *Plant J.* 89, 789–804. doi: 10.1111/tpj.13415

Cheng, S., Xian, W., Fu, Y., Marin, B., Keller, J., Wu, T., et al. (2019). Genomes of subaerial zygnematophyceae provide insights into land plant evolution. *Cell* 179, 1057–1067.e14. doi: 10.1016/j.cell.2019.10.019

Collonnier, C., Epert, A., Mara, K., Maclot, F., Guyon-Debast, A., Charlot, F., et al. (2017). CRISPR -Cas9-mediated efficient directed mutagenesis and RAD 51-dependent and RAD 51-independent gene targeting in the moss *Physcomitrella patens*. *Plant Biotechnol. J.* 15, 122–131. doi: 10.1111/pbi.12596

Concordet, J.-P., and Haeussler, M. (2018). CRISPOR: intuitive guide selection for CRISPR/Cas9 genome editing experiments and screens. *Nucleic Acids Res.* 46, W242–W245. doi: 10.1093/nar/gky354

Darriba, D., Posada, D., Kozlov, A. M., Stamatakis, A., Morel, B., and Flouri, T. (2020). ModelTest-NG: A new and scalable tool for the selection of DNA and protein evolutionary models. *Mol. Biol. Evol.* 37, 291–294. doi: 10.1093/molbev/msz189

Dhonukshe, P., Vischer, N., and Gadella, T. W. J. (2006). Contribution of microtubule growth polarity and flux to spindle assembly and functioning in plant cells. *J. Cell Sci.* 119, 3193–3205. doi: 10.1242/jcs.03048

Gibson, D. G., Young, L., Chuang, R.-Y., Venter, J. C., Hutchison, C. A., and Smith, H. O. (2009). Enzymatic assembly of DNA molecules up to several hundred kilobases. *Nat. Methods* 6, 343–345. doi: 10.1038/nmeth.1318

Gordon, D. J., Resio, B., and Pellman, D. (2012). Causes and consequences of aneuploidy in cancer. *Nat. Rev. Genet.* 13, 189–203. doi: 10.1038/nrg3123

Hamada, M., Schröder, K., Bathia, J., Kürn, U., Fraune, S., Khalturina, M., et al. (2018). Metabolic co-dependence drives the evolutionarily ancient Hydra-Chlorella symbiosis. *eLife* 7, e35122. doi: 10.7554/eLife.35122.065

Healey, A. L., Piatkowski, B., Lovell, J. T., Sreedasyam, A., Carey, S. B., Mamidi, S., et al. (2023). Newly identified sex chromosomes in the Sphagnum (peat moss) genome alter carbon sequestration and ecosystem dynamics. *Nat. Plants* 9, 238–254. doi: 10.1038/s41477-022-01333-5

Hess, S., Williams, S. K., Busch, A., Irisarri, I., Delwiche, C. F., De Vries, S., et al. (2022). A phylogenomically informed five-order system for the closest relatives of land plants. *Curr. Biol.* 32, 4473–4482.e7. doi: 10.1016/j.cub.2022.08.022

Hohe, A., Egener, T., Lucht, J. M., Holtorf, H., Reinhard, C., Schween, G., et al. (2004). An improved and highly standardised transformation procedure allows efficient production of single and multiple targeted gene-knockouts in a moss, *Physcomitrella patens. Curr. Genet.* 44, 339–347. doi: 10.1007/s00294-003-0458-4

Hori, K., Maruyama, F., Fujisawa, T., Togashi, T., Yamamoto, N., Seo, M., et al. (2014). *Klebsormidium flaccidum* genome reveals primary factors for plant terrestrial adaptation. *Nat. Commun.* 5, 3978. doi: 10.1038/ncomms4978

Horst, N. A., Katz, A., Pereman, I., Decker, E. L., Ohad, N., and Reski, R. (2016). A single homeobox gene triggers phase transition, embryogenesis and asexual reproduction. *Nat. Plants* 2, 15209. doi: 10.1038/nplants.2015.209

Hu, R., Li, X., Hu, Y., Zhang, R., Lv, Q., Zhang, M., et al. (2023). Adaptive evolution of the enigmatic Takakia now facing climate change in Tibet. Cell 186, 3558–3576.e17. doi: 10.1016/j.cell.2023.07.003

Jaillon, O., Aury, J. M., Noel, B., Policriti, A., Clepet, C., Casagrande, A., et al. (2007). The grapevine genome sequence suggests ancestral hexaploidization in major angiosperm phyla. *Nature* 449, 463–467. doi: 10.1038/nature06148

Jones, P., Binns, D., Chang, H. Y., Fraser, M., Li, W., McAnulla, C., et al. (2014). InterProScan 5: genome-scale protein function classification. *Bioinformatics* 30, 1236–1240. doi: 10.1093/bioinformatics/btu031

Katoh, K., and Standley, D. M. (2013). MAFFT multiple sequence alignment software version 7: improvements in performance and usability. *Mol. Biol. Evol.* 30, 772–780. doi: 10.1093/molbey/mst010

Kirbis, A., Rahmatpour, N., Dong, S., Yu, J., Waser, L., Huang, H., et al. (2025). Comparative analysis using a chromosome-scale genome assembly for *Funaria hygrometrica* suggests greater collinearity in mosses than in seed plants. *Commun. Biol.* 8, 330. doi: 10.1038/s42003-025-07749-x

Knosp, S., Kriegshauser, L., Tatsumi, K., Malherbe, L., Erhardt, M., Wiedemann, G., et al. (2024). An ancient role for CYP73 monooxygenases in phenylpropanoid biosynthesis and embryophyte development. EMBO J. 43, 4092–4109. doi: 10.1038/s44318-024-00181-7

Kosetsu, K., De Keijzer, J., Janson, M. E., and Goshima, G. (2013). MICROTUBULE-ASSOCIATED PROTEIN65 is essential for maintenance of phragmoplast bipolarity and formation of the cell plate in *physcomitrella patens*. *Plant Cell* 25, 4479–4492. doi: 10.1105/tpc.113.117432

Kosetsu, K., Murata, T., Yamada, M., Nishina, M., Boruc, J., Hasebe, M., et al. (2017). Cytoplasmic MTOCs control spindle orientation for asymmetric cell division in plants. *Proc. Natl. Acad. Sci. U.S.A.* 114, E8847–E8854. doi: 10.1073/pnas.1713925114

Kozgunova, E. (2025). Recent advances in plant kinetochore research. Front. Cell Dev. Biol. 12, 1510019. doi: 10.3389/fcell.2024.1510019

Kozgunova, E., and Goshima, G. (2019). A versatile microfluidic device for highly inclined thin illumination microscopy in the moss *Physcomitrella patens*. *Sci. Rep.* 9, 15182. doi: 10.1038/s41598-019-51624-9

Kozgunova, E., Nishina, M., and Goshima, G. (2019). Kinetochore protein depletion underlies cytokinesis failure and somatic polyploidization in the moss. *eLife* 8, e43652. doi: 10.7554/eLife.43652.031

Kozgunova, E., Yoshida, M. W., Reski, R., and Goshima, G. (2022). Spindle motility skews division site determination during asymmetric cell division in Physcomitrella. *Nat. Commun.* 13, 2488. doi: 10.1038/s41467-022-30239-1

Kozlov, A. M., Darriba, D., Flouri, T., Morel, B., and Stamatakis, A. (2019). RAxML-NG: a fast, scalable and user-friendly tool for maximum likelihood phylogenetic inference. *Bioinformatics* 35, 4453–4455. doi: 10.1093/bioinformatics/btz305

Kriegshauser, L., Knosp, S., Grienenberger, E., Tatsumi, K., Gütle, D. D., Sørensen, I., et al. (2021). Function of the HYDROXYCINNAMOYL-CoA: SHIKIMATE HYDROXYCINNAMOYL TRANSFERASE is evolutionarily conserved in embryophytes. *Plant Cell* 33, 1472–1491. doi: 10.1093/plcell/koab044

Kubo, M., Imai, A., Nishiyama, T., Ishikawa, M., Sato, Y., Kurata, T., et al. (2013). System for stable  $\beta$ -estradiol-inducible gene expression in the moss physcomitrella patens. *PloS One* 8, e77356. doi: 10.1371/journal.pone.0077356

Lang, D., Ullrich, K. K., Murat, F., Fuchs, J., Jenkins, J., Haas, F. B., et al. (2018). The *Physcomitrella patens* chromosome-scale assembly reveals moss genome structure and evolution. *Plant J.* 93, 515–533. doi: 10.1111/tpj.13801

Le Goff, S., Keçeli, B. N., Jeřábková, H., Heckmann, S., Rutten, T., Cotterell, S., et al. (2020). The H3 histone chaperone NASP<sup>SIM3</sup> escorts CenH3 in Arabidopsis. *Plant J.* 101, 71–86. doi: 10.1111/tpj.14518

Leong, S. Y., Yamada, M., Yanagisawa, N., and Goshima, G. (2018). SPIRAL2 stabilises endoplasmic microtubule minus ends in the moss *physcomitrella patens*. *Cell Structure Funct*. 43, 53–60. doi: 10.1247/csf.18001

Lipka, E., Herrmann, A., and Mueller, S. (2015). Mechanisms of plant cell division. WIREs Dev. Biol. 4, 391–405. doi: 10.1002/wdev.186

Liu, H.-J., Jian, L., Xu, J., Zhang, Q., Zhang, M., Jin, M., et al. (2020). High-throughput CRISPR/cas9 mutagenesis streamlines trait gene identification in maize. *Plant Cell* 32, 1397–1413. doi: 10.1105/tpc.19.00934

Liu, B., and Lee, Y.-R. J. (2022). Spindle assembly and mitosis in plants. *Annu. Rev. Plant Biol.* 73, 227–254. doi: 10.1146/annurev-arplant-070721-084258

Lopez-Obando, M., Hoffmann, B., Géry, C., Guyon-Debast, A., Téoulé, E., Rameau, C., et al. (2016). Simple and efficient targeting of multiple genes through CRISPR-cas9 in physcomitrella patens. G3 Genes|Genomes|Genetics 6, 3647–3653. doi: 10.1534/93.116.033266

Lueth, V. M., and Reski, R. (2023). Mosses. Curr. Biol. 33, R1175–R1181. doi: 10.1016/j.cub.2023.09.042

Lukowitz, W., Mayer, U., and Jürgens, G. (1996). Cytokinesis in the arabidopsis embryo involves the syntaxin-related KNOLLE gene product. *Cell* 84, 61–71. doi: 10.1016/S0092-8674(00)80993-9

Lüth, V. M., Rempfer, C., Van Gessel, N., Herzog, O., Hanser, M., Braun, M., et al. (2023). A Physcomitrella PIN protein acts in spermatogenesis and sporophyte retention. *New Phytol.* 237, 2118–2135. doi: 10.1111/nph.18691

Mao, L., Kawaide, H., Higuchi, T., Chen, M., Miyamoto, K., Hirata, Y., et al. (2020). Genomic evidence for convergent evolution of gene clusters for momilactone biosynthesis in land plants. *Proc. Natl. Acad. Sci. U.S.A.* 117, 12472–12480. doi: 10.1073/pnas.1914373117

Marchant, D. B., Chen, G., Cai, S., Chen, F., Schafran, P., Jenkins, J., et al. (2022). Dynamic genome evolution in a model fern. *Nat. Plants* 8, 1038–1051. doi: 10.1038/s41477-022-01226-7

McIntosh, J. R. (2016). Mitosis. Cold Spring Harbor Perspect. Biol. 8, a023218. doi: 10.1101/cshperspect.a023218

Meng, X., Yu, H., Zhang, Y., Zhuang, F., Song, X., Gao, S., et al. (2017). Construction of a genome-wide mutant library in rice using CRISPR/cas9.  $Mol.\ Plant\ 10,\ 1238-1241.$  doi: 10.1016/j.molp.2017.06.006

Menges, M., and Murray, J. A. H. (2002). Synchronous *Arabidopsis* suspension cultures for analysis of cell-cycle gene activity. *Plant J.* 30, 203–212. doi: 10.1046/j.1365-313X.2002.01274.x

Merchant, S. S., Prochnik, S. E., Vallon, O., Harris, E. H., Karpowicz, S. J., Witman, G. B., et al. (2007). The Chlamydomonas genome reveals the evolution of key animal and plant functions. *Science* 318, 245–251. doi: 10.1126/science.1143609

Miki, T., Naito, H., Nishina, M., and Goshima, G. (2014). Endogenous localizome identifies 43 mitotic kinesins in a plant cell. *Proc. Natl. Acad. Sci. U.S.A.* 111, E1053–E1061. doi: 10.1073/pnas.1311243111

Miki, T., Nakaoka, Y., and Goshima, G. (2016). "Live cell microscopy-based RNAi screening in the moss physcomitrella patens," in *High-throughput RNAi screening: methods and protocols. Methods Mol. Biol.* (New York, NY: Humana Press), 225–246.

Moody, L. A. (2022). Unravelling 3D growth in the moss *Physcomitrium patens*. Essays Biochem. 66, 769–779. doi: 10.1042/EBC20220048

Mueller, S. J., Lang, D., Hoernstein, S. N. W., Lang, E. G. E., Schuessele, C., Schmidt, A., et al. (2014). Quantitative analysis of the mitochondrial and plastid proteomes of the moss *physcomitrella patens* reveals protein macrocompartmentation and microcompartmentation. *Plant Physiol.* 164, 2081–2095. doi: 10.1104/pp.114.235754

Nakaoka, Y., Miki, T., Fujioka, R., Uehara, R., Tomioka, A., Obuse, C., et al. (2012). An inducible RNA interference system in *physcomitrella patens* reveals a dominant role of augmin in phragmoplast microtubule generation. *Plant Cell* 24, 1478–1493. doi: 10.1105/tpc.112.098509

Nishiyama, T., Sakayama, H., de Vries, J., Buschmann, H., Saint-Marcoux, D., Ullrich, K. K., et al. (2018). The chara genome: secondary complexity and implications for plant terrestrialization. *Cell* 174, 448–464.e24. doi: 10.1016/j.cell.2018.06.033

Nystedt, B., Street, N. R., Wetterbom, A., Zuccolo, A., Lin, Y. C., Scofield, D. G., et al. (2013). The Norway spruce genome sequence and conifer genome evolution. *Nature* 497, 579–584. doi: 10.1038/nature12211

Ødum, M. T., Teufel, F., Thumuluri, V., Armenteros, J. J. A., Johansen, A. R., Winther, O., et al. (2024). DeepLoc 2.1: multi-label membrane protein type prediction using protein language models. *Nucleic Acids Res.* 52, W215–W220. doi: 10.1093/nar/gkae237

Ouyang, S., Zhu, W., Hamilton, J., Lin, H., Campbell, M., Childs, K., et al. (2007). The TIGR Rice Genome Annotation Resource: improvements and new features. *Nucleic Acids Res.* 35, D883–D887. doi: 10.1093/nar/gkl976

Perroud, P., Haas, F. B., Hiss, M., Ullrich, K. K., Alboresi, A., Amirebrahimi, M., et al. (2018). The *Physcomitrella patens* gene atlas project: large-scale RNA -seq based expression data. *Plant J.* 95, 168–182. doi: 10.1111/tpj.13940

Polle, J. E. W., Barry, K., Cushman, J., Schmutz, J., Tran, D., Hathwaik, L. T., et al. (2017). Draft nuclear genome sequence of the halophilic and beta-carotene-accumulating green alga *dunaliella salina* strain CCAP19/18. *Genome Announcements* 5, e01105–e01107. doi: 10.1128/genomeA.01105-17

Pressel, S., Ligrone, R., and Duckett, J. G. (2008). Cellular differentiation in moss protonemata: A morphological and experimental study. *Ann. Bot.* 102, 227–245. doi: 10.1093/aob/mcn080

Price, M. N., Dehal, P. S., and Arkin, A. P. (2010). FastTree 2–approximately maximum-likelihood trees for large alignments. *PloS One* 5, e9490. doi: 10.1371/journal.pone.0009490

Price, D. C., Goodenough, U. W., Roth, R., Lee, J. H., Kariyawasam, T., Mutwil, M., et al. (2019). Analysis of an improved *Cyanophora paradoxa* genome assembly. *DNA Res.* 26, 287–299. doi: 10.1093/dnares/dsz009

R Core Team (2024). R: A Language and Environment for Statistical Computing. Vienna, Austria: R Foundation for Statistical Computing. Available online at: https://www.R-project.org/ (Accessed March 01, 2024).

Prochnik, S. E., Umen, J., Nedelcu, A. M., Hallmann, A., Miller, S. M., Nishii, I., et al. (2010). Genomic analysis of organismal complexity in the multicellular green alga *Volvox carteri. Science* 329, 223–226. doi: 10.1126/science.1188800

Ranawaka, B., An, J., Lorenc, M. T., Jung, H., Sulli, M., Aprea, G., et al. (2023). A multi-omic *Nicotiana benthamiana* resource for fundamental research and biotechnology. *Nat. Plants* 9, 1558–1571. doi: 10.1038/s41477-023-01489-8

Rasmussen, C. G., and Bellinger, M. (2018). An overview of plant division-plane orientation. *New Phytol.* 219, 505–512. doi: 10.1111/nph.15183

Rensing, S. A., Goffinet, B., Meyberg, R., Wu, S.-Z., and Bezanilla, M. (2020). The moss *physcomitrium (Physcomitrella) patens*: A model organism for non-seed plants. *Plant Cell* 32, 1361–1376. doi: 10.1105/tpc.19.00828

Resemann, H. C., Herrfurth, C., Feussner, K., Hornung, E., Ostendorf, A. K., Gömann, J., et al. (2021). Convergence of sphingolipid desaturation across over 500 million years of plant evolution. *Nat. Plants* 7, 219–232. doi: 10.1038/s41477-020-0884-3.

Reski, R. (2018a). Enabling the water-to-land transition. Nat. Plants 4, 67-68. doi: 10.1105/tpc.19.00828

Reski, R. (2018b). Quantitative moss cell biology. Curr. Opin. Plant Biol. 46, 39–47. doi: 10.1016/j.pbi.2018.07.005

Romeiro Motta, M., Nédélec, F., Saville, H., Woelken, E., Jacquerie, C., Pastuglia, M., et al. (2024). The cell cycle controls spindle architecture in Arabidopsis by activating the augmin pathway. *Dev. Cell* 59, 2947–2961.e9. doi: 10.1016/j.devcel.2024.08.001

Rossoni, A. W., Price, D. C., Seger, M., Lyska, D., Lammers, P., Bhattacharya, D., et al. (2019). The genomes of polyextremophilic cyanidiales contain 1% horizontally transferred genes with diverse adaptive functions. *eLife* 8, e45017. doi: 10.7554/eLife.45017

Sablowski, R., and Gutierrez, C. (2022). Cycling in a crowd: Coordination of plant cell division, growth, and cell fate. *Plant Cell* 34, 193–208. doi: 10.1093/plcell/koab222

Sinclair, R., Hsu, G., Davis, D., Chang, M., Rosquete, M., Iwasa, J. H., et al. (2022). Plant cytokinesis and the construction of new cell wall. *FEBS Lett.* 596, 2243–2255. doi: 10.1002/1873-3468.14426

Slane, D., Kong, J., Berendzen, K. W., Kilian, J., Henschen, A., Kolb, M., et al. (2014). Cell type-specific transcriptome analysis in the early *Arabidopsis thaliana* embryo. *Development* 141, 4831–4840. doi: 10.1242/dev.116459

Smertenko, A., Hewitt, S. L., Jacques, C. N., Kacprzyk, R., Liu, Y., Marcec, M. J., et al. (2018). Phragmoplast microtubule dynamics – a game of zones. *J. Cell Sci.* 131, jcs203331. doi: 10.1242/jcs.203331

Sperschneider, J., Catanzariti, A. M., Deboer, K., Petre, B., Gardiner, D. M., Singh, K. B., et al. (2017). LOCALIZER: subcellular localization prediction of both plant and effector proteins in the plant cell. *Sci. Rep.* 7, 44598. doi: 10.1038/srep44598

Sreedasyam, A., Plott, C., Hossain, M. S., Lovell, J. T., Grimwood, J., Jenkins, J. W., et al. (2023). JGI Plant Gene Atlas: an updateable transcriptome resource to improve functional gene descriptions across the plant kingdom. *Nucleic Acids Res.* 51, 8383–8401. doi: 10.1093/nar/ekad616

Teufel, F., Almagro Armenteros, J. J., Johansen, A. R., Gíslason, M. H., Pihl, S. I., Tsirigos, K. D., et al. (2022). SignalP 6.0 predicts all five types of signal peptides using protein language models. *Nat. Biotechnol.* 40, 1023–1025. doi: 10.1038/s41587-021-01156-3

Traas, J., Bellini, C., Nacry, P., Kronenberger, J., Bouchez, D., and Caboche, M. (1995). Normal differentiation patterns in plants lacking microtubular preprophase bands. *Nature* 375, 676–677. doi: 10.1038/375676a0

Tuskan, G. A., DiFazio, S., Jansson, S., Bohlmann, J., Grigoriev, I., Hellsten, U., et al. (2006). The genome of black cottonwood, *Populus trichocarpa* (Torr. & Gray). *Science* 313, 1596–1604. doi: 10.1126/science.1128691

Whitfield, M. L., Sherlock, G., Saldanha, A. J., Murray, J. I., Ball, C. A., Alexander, K. E., et al. (2002). Identification of genes periodically expressed in the human cell cycle and their expression in tumors. *Mol. Biol. Cell* 13, 1977–2000. doi: 10.1091/mbc.02-02-0030

Wright, A. J., Gallagher, K., and Smith, L. G. (2009). discordia1 and alternative discordia1 Function Redundantly at the Cortical Division Site to Promote Preprophase Band Formation and Orient Division Planes in Maize. *Plant Cell* 21, 234–247. doi: 10.1105/tpc.108.062810

Wu, S.-Z., and Bezanilla, M. (2014). Myosin VIII associates with microtubule ends and together with actin plays a role in guiding plant cell division. eLife 3, e03498. doi: 10.7554/eLife.03498.035

Yamada, M., and Goshima, G. (2017). Mitotic spindle assembly in land plants: molecules and mechanisms. *Biol. (Basel)* 6, 6. doi: 10.3390/biology6010006

Yamada, M., Matsuyama, H. J., Takeda-Kamiya, N., Sato, M., and Toyooka, K. (2025). Class II kinesin-12 facilitates cell plate formation by transporting cell plate materials in the phragmoplast. *Nat. Plants* 11, 340–358. doi: 10.1038/s41477-025-01909-x

Yamada, M., Miki, T., and Goshima, G. (2016). "Imaging mitosis in the moss physcomitrella patens," In P. Chang and R. Ohi (eds) *The Mitotic Spindle. Methods Mol. Biol.* (New York, NY: Humana Press), 1413. doi: 10.1007/978-1-4939-3542-0\_17

Ye, N., Han, W., Toseland, A., Wang, Y., Fan, X., Xu, D., et al. (2022). The role of zinc in the adaptive evolution of polar phytoplankton. *Nat. Ecol. Evol.* 6, 965–978. doi: 10.1038/s41559-022-01750-x

Yi, P., and Goshima, G. (2022). Division site determination during asymmetric cell division in plants. *Plant Cell* 34, 2120–2139. doi: 10.1093/plcell/koac069

Yin, Z., Gan, Y., Chen, Y., Kozgunova, E., and Yi, P. (2025). The microtubule cytoskeleton in bryophytes. Cytoskeleton~0,~1-28.~doi:~10.1002/cm.22009

Yoshida, M. W., and Kozgunova, E. (2023). "Microfluidic device for high-resolution cytoskeleton imaging and washout assays in *physcomitrium* (Physcomitrella) *patens*,"

In P. J. Hussey and P. Wang (eds) *The Plant Cytoskeleton. Methods Mol. Biol.*, (New York, NY: Humana Press), 2604. doi: 10.1007/978-1-0716-2867-6\_11

Yu, G., Smith, D. K., Zhu, H., Guan, Y., and Lam, T. T. Y. (2017). ggtree: an r package for visualization and annotation of phylogenetic trees with their covariates and other associated data. *Methods Ecol. Evol.* 8, 28–36. doi: 10.1111/2041-210X 12628

Zhang, J., Feng, C., Su, H., Liu, Y., Liu, Y., and Han, F. (2020a). The cohesin complex subunit zmSMC3 participates in meiotic centromere pairing in maize. *Plant Cell* 32, 1323–1336. doi: 10.1105/tpc.19.00834

Zhang, J., Fu, X. X., Li, R. Q., Zhao, X., Liu, Y., Li, M. H., et al. (2020b). The hornwort genome and early land plant evolution. Nat. Plants 6, 107–118. doi: 10.1038/s41477-019-0588-4